Deltares

Vibration measurements by Distributed Acoustic Sensing

Interpretation results feasibility study

Vibration measurements by Distributed Acoustic Sensing
Interpretation results feasibility study

Client	Deltares
Contact	Ing. H.A. Aantjes
Reference	SO2020 Enabling technologies / future sensing
Keywords	Field test, fibre optics, accelerometers, vibrations, validation

Document control	
Version	1.0
Date	06-02-2024
Project nr.	11205308-002
Document ID	11205308-002-BGS-0001
Pages	57
Status	Final

Author(s)		
	Dr. E. Obando Hernandez	
	Dr. P. Hölscher	

Summary

In December 2019, Deltares carried out a field test where green field vibrations from several sources were measured by both accelerometers as well a buried glass-fibre. The final target of the work is to determine the possibility to use glass fibres in the soil to measure vibration levels and the expected accuracy. This report gives a preliminary comparison of the results.

This report contains a literature review on the subject, the development of basic technics to process the registered fibre optics data and the comparison of the results from fibre optics measurements with traditional accelerometers.

It is concluded that the results of each equipment show good similarity. This means that the applicability of fibre optics for soil identification seems possible. The application of fibre optics for traditional vibration measurements where an accurate determination of the maximum value is essential, requires further research.

Contents

	Summary	**4**
1	**Introduction**	**7**
1.1	Background of the project	7
1.2	Description of the project	7
2	**Objectives and structure of report**	**8**
2.1	Objectives	8
2.2	Structure of the report	8
3	**Distributed acoustic sensing DAS – Basics and literature review**	**9**
3.1	Fundamentals of distributed acoustic sensing	9
3.2	Converting strain to particle velocity	10
3.3	Previous studies	10
3.3.1	Earthquake monitoring	10
3.3.2	Shallow ground characterization	13
3.3.3	Borehole seismic applications	16
3.3.4	Converting DAS to equivalent velocity geophone signal	17
4	**Data acquisition**	**20**
4.1	Survey site description	20
4.2	Field set-up	21
4.3	Description of acquisition system	23
4.3.1	Intelligent Distributed acoustic sensing	23
4.3.2	Acoustic bandwidth and dynamic range	24
4.3.3	Spatial resolution and measuring range	24
4.4	Field data acquisition	25
4.4.1	Acquisition parameters	25
5	**Data processing**	**27**
5.1	Data-base preparation	27
5.2	Data pre-processing	28
6	**Results for vibration levels**	**30**
6.1	Frequency domain analysis of DAS and Accelerometer signals	30
6.2	Time domain analysis of collected DAS and Accelerometer signals	33
6.2.1	Vertical Impactor source	34
6.2.2	Sledge-hammer source	36
6.2.3	Amplitude attenuation	39
6.2.4	Coiled sections	40
6.3	Velocity – to – strain ratio from accelerometers and DAS signals	41
6.4	Effect of coupling conditions for all fibre optic segments	43
6.5	Equivalent geophone time-history velocity signal	44
7	**Results for surface wave analysis**	**47**
7.1	Active surface waves	47
7.2	Passive surface waves	49
7.3	Velocity structure at the test site	50

8	**Discussion**	**53**
	Conclusions	**54**
	References	**55**
	Appendix	**56**

1 Introduction

1.1 Background of the project

Deltares has been working to provide insights into the risks and uncertainties of engineering parameters of the subsurface along railway throughout Netherlands. Joint projects are being carried out into vibration monitoring and the stability of earth tracks. In recent years efforts have been focused on the validation of the rail gradation predictions using the measurement train data.

Because of this increasing physical load on the track and track body, the quality is put under pressure resulting on the modification of designed strength parameters. More and heavier trains also influence vibrations to the environment. Sometimes these vibrations are felt and can affect the people and buildings in the rail zones. The subsurface plays a major role in this, but at the same time it is an uncertain factor of which insufficient is known.

Currently, an innovative technique that promises a high-density information in the spatial and temporal domain, is the Distributed Acoustic systems (DAS) that uses fibre optics cable buried under the ground. Several publications have reported the benefits and potential of this innovative technology, especially because fibre optics cables used for telecommunication purposes are buried underground almost everywhere, which offers the possibility to map the response of physical properties of the ground.

1.2 Description of the project

Despite the great potential of DAS, little is known about its real capabilities to reproduce similar or equivalent information to traditional vibration monitoring systems. To assess the potential of DAS as a vibration device to characterize the level of vibrations from different types of sources including induced by trains, road traffic, and construction machines, the sensitivity of buried fibre optics cables like the ones comprising telecommunication networks need to be tested.

In this project we carried out an experiment that consists of a comparative analysis of the collected records using various types of energy sources, including ambient background noise using both fibre optics and conventional accelerometers. This experiment will help to quantitatively determine, how well the vibration characteristics can be realistically evaluated using DAS systems.

This report is a preliminary study on the results of the signals gathered in the field test. It whether the quality of the signals is enough to state that the target of the field test is reached and to get some initial ideas for further elaboration. Due to budget limitations a full elaboration of the large amount of data was not yet possible in 2020. Further elaboration is foreseen for next years.

2 Objectives and structure of report

2.1 Objectives

For this field experiment the main objective is collecting field data using glass fibre measurements and conventional acquisition systems.

Thus, the main objective is to assess the similarities and differences among strain-rate and acceleration/velocity data in frequency and time domain when using impulsive active type sources.

Additional questions to be answered are:

a) To analyse the potential influence on using spatial sampling and the gauge length during the DAS data acquisition.
b) To analyse the differences from signals collected using coiled and linear fibre optics cables.
c) To assess the effect of coupling of DAS signals in frequency domain considering various fibre configurations.

Since the field test could be easily extended with a string with Geophones as used by Deltares for MASW tests, this extension has been made. The additional question it the assessment of the reliability of the dispersion properties retrieved from the collected DAS wavefield when using both active and passive source types. This part will be discussed limitedly.

2.2 Structure of the report

We have started the research with a short literature review on existing methods applied for determination of vibrations from fibre optic measurements. The data acquisition and data processing are described in the two following Chapters 4 and 5.

The comparison of the results by Fibre Optics and traditional methods is described in the next two Chapters Chapter 6 describes the results for vibration levels (comparison with measurements with the accelerometers). Chapter 7 describes the results for the surface wave analysis (comparison with the results from the geophone string).

3 Distributed acoustic sensing DAS – Basics and literature review

3.1 Fundamentals of distributed acoustic sensing

The use of Fibre optics cable as acoustic sensor has emerged as an alternative to record the incoming acoustic wavefield for several engineering and geophysical applications (Daley, Miller, Dodds, Cook, & Freifeld, 2016); Shragge et al. (2019); (Wang et al., 2018).

The DAS interrogator passes the backscattered light over a fixed distance (gauge length) dx along the fiber, centred at position x through optical components that create a coherent interference signal. The DAS response is linearly proportional to the average fibre elongation over the gauge length. The DAS optical signal processing is designed to extract for each sampling interval (user selected), the change in fibre strain with respect to the previous temporal sampling interval at that channel.

In the DAS native data format, each digital sample is indexed by the centre location of a moving window along a cable's fibre core and recording time (Daley et al., 2016). Thus, if in Figure 3.1, $u(x,t)$ represents the dynamic displacement *u(x,t)* of the fibre (DAS_{values}) at axial location x and time t.

$$\boldsymbol{DAS_{values}} = \frac{\left[u\left(x+\frac{dx}{2},\ t+dt\right)-u\left(x-\frac{dx}{2},t+dt\right)\right]}{dxdt} - \frac{\left[u\left(x+\frac{dx}{2},t\right)-u\left(x-\frac{dx}{2},t\right)\right]}{dxdt} \qquad \text{Eq. 3-1}$$

Where dx and dt are the spatial gauge length and temporal sample interval respectively.

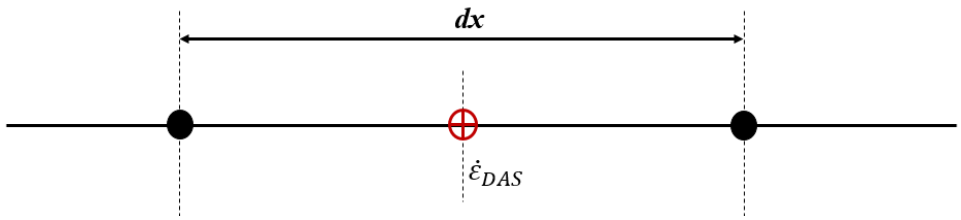

Figure 3.1. Sampling interval along a gauge length, dx.

By rewriting Eq. 3-1 and after division by the gauge length and sample interval we find:

$$\boldsymbol{DAS_{values}} = \frac{\left[u\left(x+\frac{dx}{2},\ t+dt\right)-u\left(x-\frac{dx}{2},t+dt\right)\right]}{dxdt} - \frac{\left[u\left(x+\frac{dx}{2},t\right)-u\left(x-\frac{dx}{2},t\right)\right]}{dxdt} = \frac{d\varepsilon}{dt} = \dot{\varepsilon} \qquad \textbf{Eq. 3-2}$$

Obviously, the DAS interrogator returns the strain rate $\dot{\varepsilon}$. The strain as a function of time can be found by integration.

$$\boldsymbol{\varepsilon(x,t) = \int_0^t \dot{\varepsilon}\,(x,t)dt} \qquad \text{Eq. 3-3}$$

This means that the strain is always measured relative to the initial position where the measurement of DAS_{values} start at.

3.2 Converting strain to particle velocity

A harmonic wave propagating in the x-direction is defined by *Eq. 3-4*. .A plane harmonic wave is defined by A(x) is constant.

$$u(x,t) = A(x)e^{i(kx-\omega t)} \qquad \textbf{Eq. 3-4}$$

The particle velocity and strain obtained from DAS is related using the following expression (*Eq. 3-5*):

$$\varepsilon = \frac{\partial u}{\partial x} = \pm\frac{1}{c}\frac{\partial u}{\partial t} = \pm\frac{1}{c}\dot{u} \qquad \textbf{Eq. 3-5}$$

Where c is the apparent phase velocity in the material. ${}^{1}\!/_{c} = {}^{k}\!/_{\omega}$ is the apparent slowness of the plane wave along the fibre direction, and $\frac{\partial u}{\partial t} = \dot{u}$, is the particle velocity as measured with conventional nodal receiver. The particle velocity is computed utilizing ***Eq. 3-5***:

$$\dot{u} = \varepsilon * c \qquad \textbf{Eq. 3-6}$$

3.3 Previous studies

A short literature review that comprises the most recent and relevant publications of DAS applications, in wide band frequency response, is presented. Some of the most popular applications are related to earthquake monitoring, shallow ground characterization and borehole seismic.

3.3.1 Earthquake monitoring

Wang demonstrated the reliability of DAS signals to provide accurate and physically meaningful information for earthquake monitoring purposes (Wang et al., 2018). Figure 3.2 shows an example of a collected waveform from the Hawthorne earthquake occurred in March 2016, where clear P and S-wave patterns are identified. The collected waveforms appear in good agreement with recorded waveforms, for the same event, collected with standard nodal receivers.

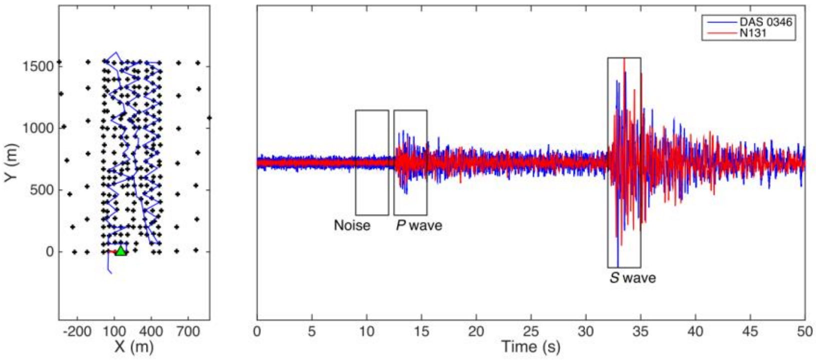

Figure 3.2. *Example comparison of normalized DAS strain rate (blue) and raw geophone coil-case velocity (red) records for 2016 March 21 Hawthorne earthquake. Boxes show the 2 s time windows that were used to obtain noise and signal for P-and S-wave arrivals. The geophone record was scaled to match its peak amplitude to that of DAS. The inset map shows location of DAS segment (red line) and geophone (green triangle).(Wang et al., 2018).*

In the literature, several tailored made fiber optic arrays have been installed by experiments purposes. Figure 3.3a shows three test sites located at the Research and Engineering Laboratory in Fairbanks Permafrost station where a grid of Fibre optic cables was installed in ditches of 20 cm. The L-shape array of fiber optics buried in 50 cm trench installed at the Richmond field station in northern California (Figure 3.3b).

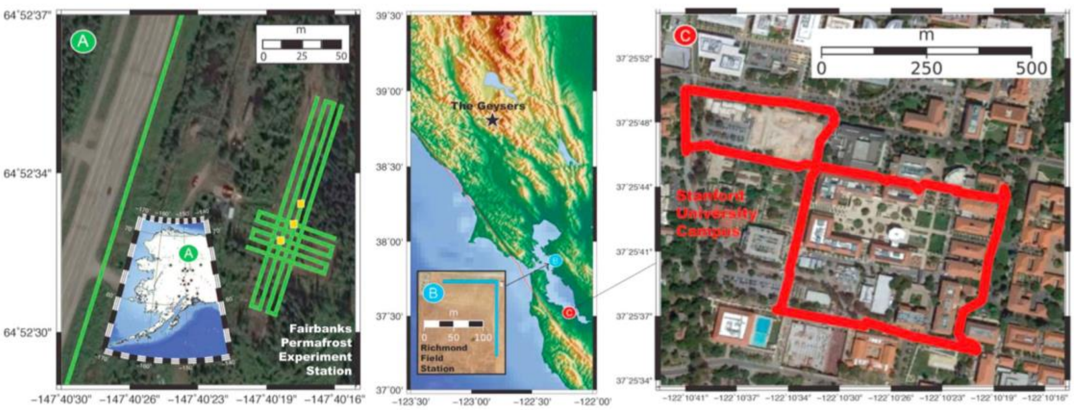

Figure 3.3. *Color-coded maps of the fiber-optic arrays used for the experiments at (a) the Fairbanks Permafrost Experiment Station, AK, (b) Richmond Field Station, CA, and (c) Stanford University, CA. Colored lines indicate fiber cables directly installed in shallow trenches or conduit.*

An example Fairbanks DAS array recording of the 26 August 2016 M3.8 Central Alaska earthquake (distance =150 km) is displayed in Figure 3.4a. The fiber optic line was installed in a shallow trench of 160 m at every 1 m with a gauge length of 10 m. Figure 3.4b displays the Fourier Amplitude Spectra from the earthquake signal (thick lines) compared with a background noise window (thin lines) measured by a single DAS channel (red) and the 10-channel DAS stack.

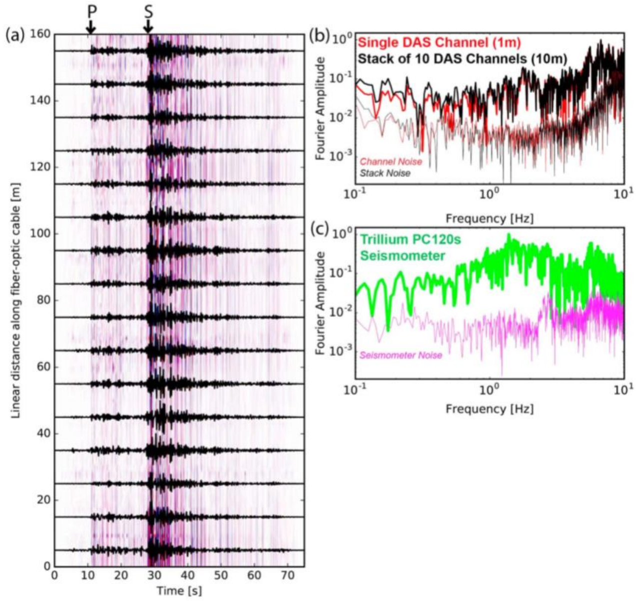

Figure 3.4. (a) Silixa iDAS data recorded with a single-mode fiber-optic cable (b) DAS Fourier amplitude spectra Spectra are normalized to the single DAS channel peak signal value. (c) Signal and noise for the horizontal channel of a collocated Trillium Posthole Compact 120 s inertial seismometer. All Spectra amplitudes are normalized. (Lindsey et al., 2017).

An earthquake record collected on 8 April 2016 M3.8 Geysersat the Richmond site, allowed the computation of the propagation back azimuth and slowness of the seismic wavefield (Figure 3.5). The collected wavefield consisted of 192 traces at every 1.0 meter with clear definition of P and S-wave arrivals. The recorded collected where bandpass filtered between 0.25 – 1.0 Hz.

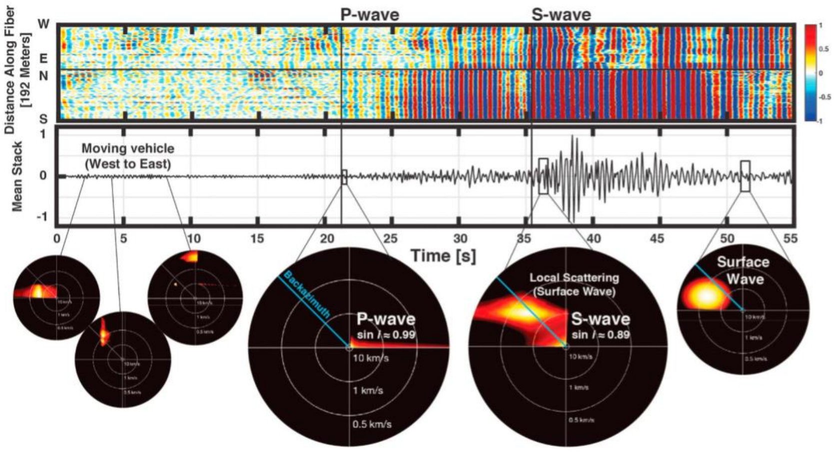

Figure 3.5. Beamforming the 8 April 2016 M3.8 Geysers, CA, earthquake observation on the Richmond, CA, DAS array. (top) The full 192 seismic array recording shown in Figure 1b from west-east and then north-south. Bandpass filter is in the range 0.25 – 1 Hz. (middle) Stack of the seismic array records shown. (bottom) Polar diagrams showing the peak beam as a function of back-azimuth and slowness for different windowed times (Lindsey et al., 2017)

The conclusion is that literature suggests that a fibre optics measurement can be used to derive the strength of an earthquake wave. Section 3.3.4 will discuss the methodology that was used to calculate from strain to velocity.

3.3.2 Shallow ground characterization

DAS implementation has been also utilized for ground characterisation by means of surface wave analysis using both active and passive survey types. Successful examples of passive surveys using DAS systems, demonstrate the reliability of retrieved ambient noise records to compute the dispersion properties of the ground structure. Dou et al., (2017), performed an experimental study using an L-shape cable set-up (100 m -- EW and 110 m -- NS). Fibre optic cables were buried in trenches of 0.5 m depth and 0.1 m width. Ambient noise measurements were performed continuously for three weeks using 1000 Hz of sampling frequency. The dataset consisted of 2.7 Terabytes of data (separated in individual files of 60-seconds duration). The effective length excluding bended segments were 97 m and 94 m in the EW and NS directions respectively.

From collected ambient noise records virtual active-like shot gather were computed using a cross-correlation procedure with 60 seconds time window. The computed virtual shot gathers were utilized to retrieve the dispersion properties of the soil underneath. Figure 3.6 depicts the average computed phase-velocity-spectrum and the inverted S-wave velocity profiles using a multimodal approach (Dou et al., 2017). They concluded that the 24-hours ambient noise data secures the stability of Vs – profile at the top 20 meters, with a repeatability of 2% ($\Delta V_S / V_S$).

Dou et al., (2017), also analysed the effect of the cable packaging of fibre optics cable in the strength of the collected wavefield in time and frequency domain. Figure 3.7 depicts the waveforms (60-seconds time window) and average spectral shape of fibre optic cables with different packaging characteristics available in the market. It is observed that the spectral shape is very similar and consistent in the frequency range of 0.6 Hz – 37 Hz.

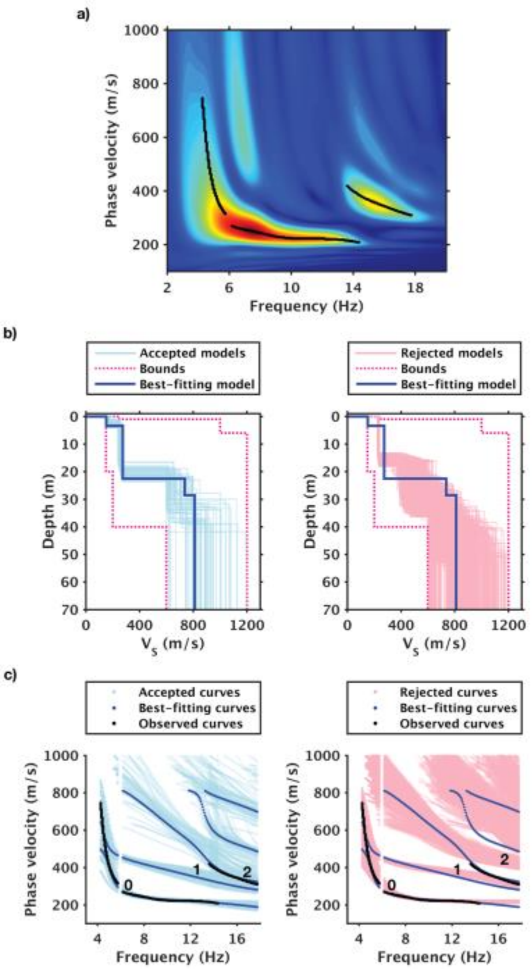

Figure 3.6. Dispersion measurement and inversion results of a 24-hour stack. (a) Dispersion measurements. (b) Top 0.1% best-fit models. (c) Observed and model-predicted (using profiles shown in (b)) dispersion curves. (Dou et al., 2017).

Thus, they concluded that cable packaging exerts very little effect on the collected signals. So, when deciding the type of single mode to be used, the factor main factor to be considered are cost, durability, and practical aspects during the installation.

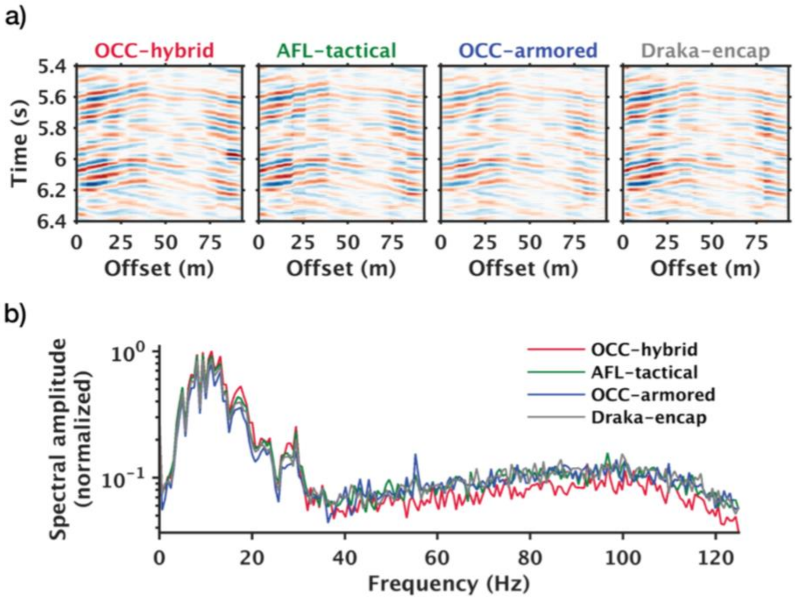

Figure 3.7. (a) Zoom-in view of 1-second noise records. (b) Mean spectral amplitudes computed using identical spatial and temporal windows.(Dou et al., 2017).

DAS offers an enormous potential of utilizing existing unused telecommunication fibre optics network, also known as dark fiber. Dark fiber may provide a unique tool to investigate the subsurface soil conditions in urban areas where the use standard geophysical surveys is often prohibited (Ajo-Franklin et al., 2019; Dou et al., 2017; Parker et al., 2014; Shragge et al., 2019; Tribaldos et al.; Wang et al., 2018).

Ajo-Frankling et al., (2019) utilized a segment of the Dark fiber testebed network of 20,920 km design to test novel network communication equipment and protocols (*Figure 3.8*). The selected segment goes from West Sacramento, California to Woodland California. The selected fiber (blue) is approximately co-linear with an active railways. The data collection system utilized was an iDAS interrogator from Silixa, using 500 Hz of sampling frequency, spatial sampling of 2.0 m and gauge length of 10.0 m. An important task is to stablish the geometry of the survey line which requires placing GPS reference points by delivering impacts along the fiber line. The fiber segment of analysis was of 6600 m long (*Figure 3.8*b).

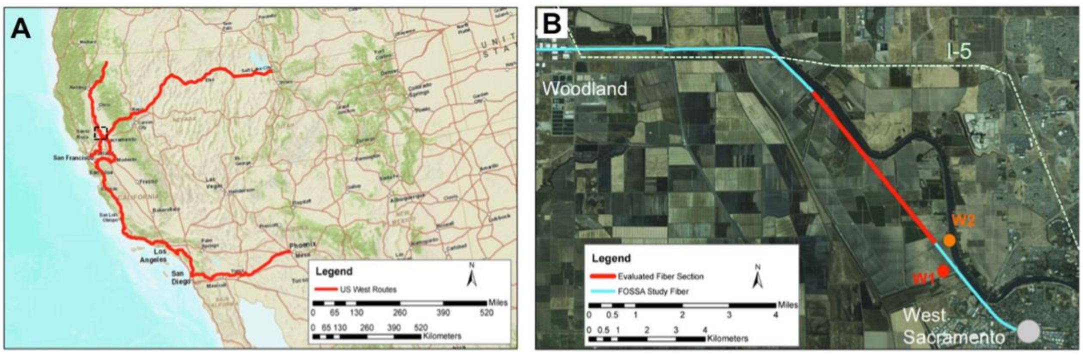

Figure 3.8. (A) The regional network within CA and western NV and (B) The subsection of the network of 6600 m utilized for the analysis (thick red line). (Ajo-Franklin et al., 2019).

Ambient noise measurements (in a frequency range of 2 – 30 Hz) were cross-correlated to compute virtual active-like shot-gathers (for consecutive shot-gathers of 120 m -- 61 traces) to compute the dispersion image using MASW wavefield transformation method. Consecutive 1D velocity profiles were utilized to compute a 2D S-wave cross section along the survey line. For the 2D cross-sections only 57% of the survey line (6600 m) that is 3760 m, is utilized (Figure 3.9). The gaps observed (Figure 3.9a) in the cross-section corresponds (that is the 43% not considered) corresponds to unclear dispersion patterns associated to bad coupling of the fiber line or strong coherent directional noise from localized sources.

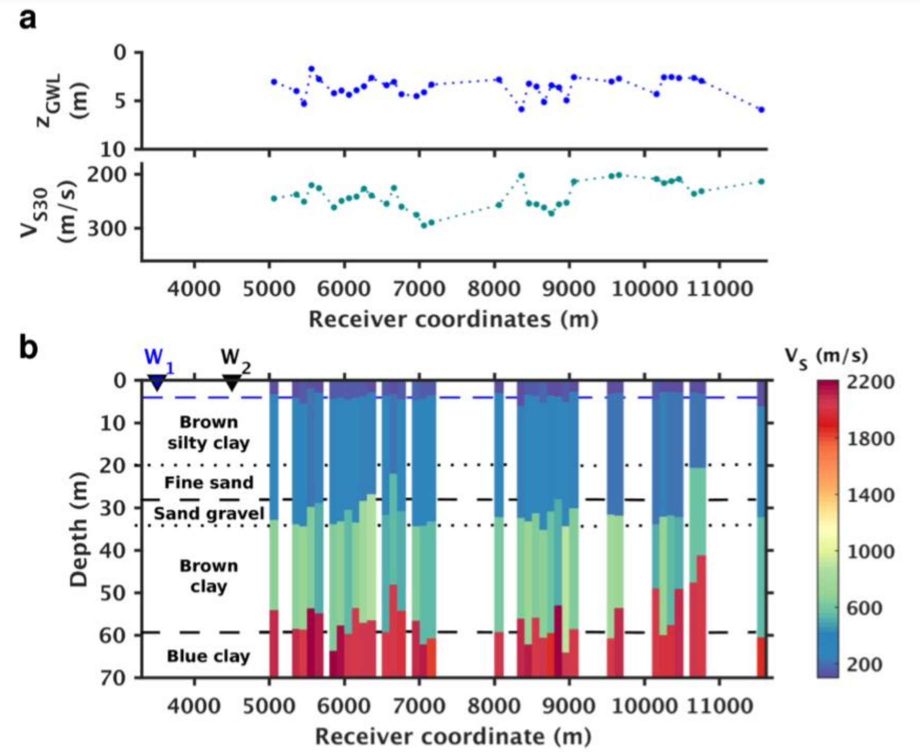

Figure 3.9. Shear-wave velocity (Vs) inversion results and ground truth comparison. (a) Depths of groundwater levels (GWL) (upper) and Vs30 estimates (lower) extracted from the surface wave inversion results. (b) Pseudo-color display of Vs profiles and comparisons against well data.

3.3.3 Borehole seismic applications

During the past few years, DAS measurements have become in a popular and accurate geophysical tool for borehole seismic surveys in gas and oil applications. Besides its implementation in vertical seismic profiling (VSP) surveys for velocity structure determination (Figure 3.10), iDAS has been successfully utilized to measure acoustic signals due to hydromechanical response of individual fractures caused by hydraulic stresses, aquifer heterogeneities, and the interconnectivity between wells (Bakku, 2015; Daley et al., 2016).

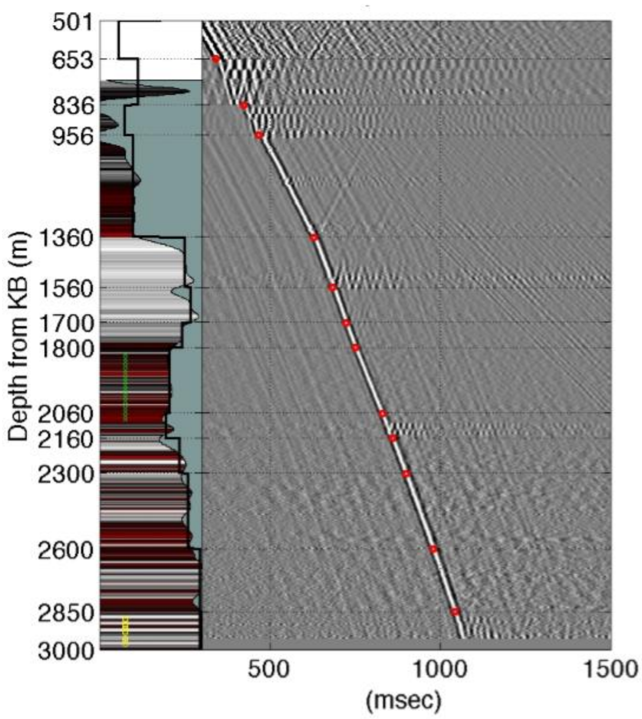

Figure 3.10. The far-left panel, which is coloured by gamma-ray log data, shows local velocities and a blocked velocity model (thick black line) which were both derived from picked DAS first arrival times. Depths associated with major velocity changes in the DAS data are indicated with red dots. (Daley et al., 2016).

3.3.4 Converting DAS to equivalent velocity geophone signal

Although the evidence suggests the great potential of DAS to be considered a reliable alternative for both, either ground characterization (Ajo-Franklin et al., 2019) and in earthquake monitoring (Lindsey et al., 2017; Wang et al., 2018), it is not clear to what extent DAS signals offers improved resolution and accurate in both time and frequency domain respect to traditional nodal high quality sensors.

To offer more insights on the similarities of collected DAS acoustic signals the collected waveforms must be compared using a common physical unit representation. Wang et al., (2018) compared collected DAS and geophone signals in terms of strain and particle velocity. The particle velocity of geophone signals was converted to strain utilizing the computed apparent velocity from observed first arrivals.

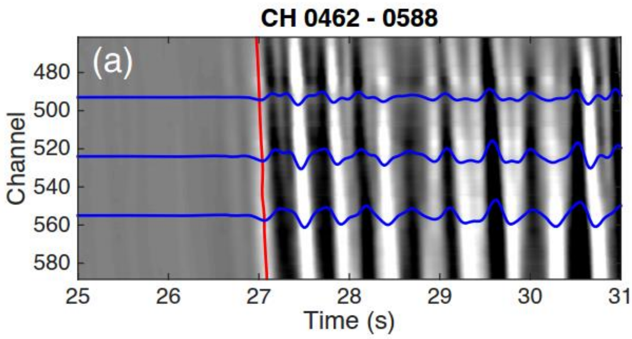

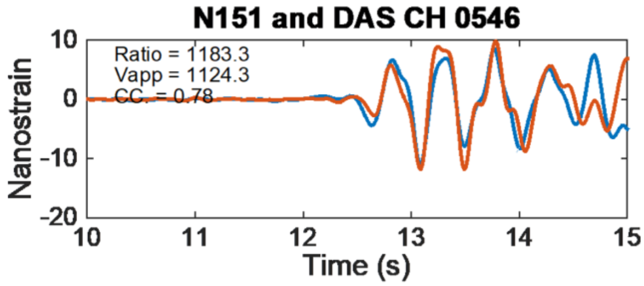

Figure 3.11.(top) apparent velocity computed using P-wave arrivals; (bottom) strain amplitudes of collected waveforms.

Figure 3.11 (bottom) shows an example of the pair of converted DAS and geophone signals. The local velocity utilized that is of 1124.3 m/sec corresponds to the apparent velocity displayed in Figure 3.11 (top).

These results lead to some remarks:

- Using the apparent P-wave speed give reasonable results for vibration level of the P waves.
- From Figure 3.11 (top) it cannot be concluded that the value of the calculated velocity is correct.
- The main period in the signals is about 0.5 s. With the apparent wave speed of about 1100 m/s this leads to wavelength of 550 m. This differs strongly from the values that is typical for soft soil civil engineering applications.

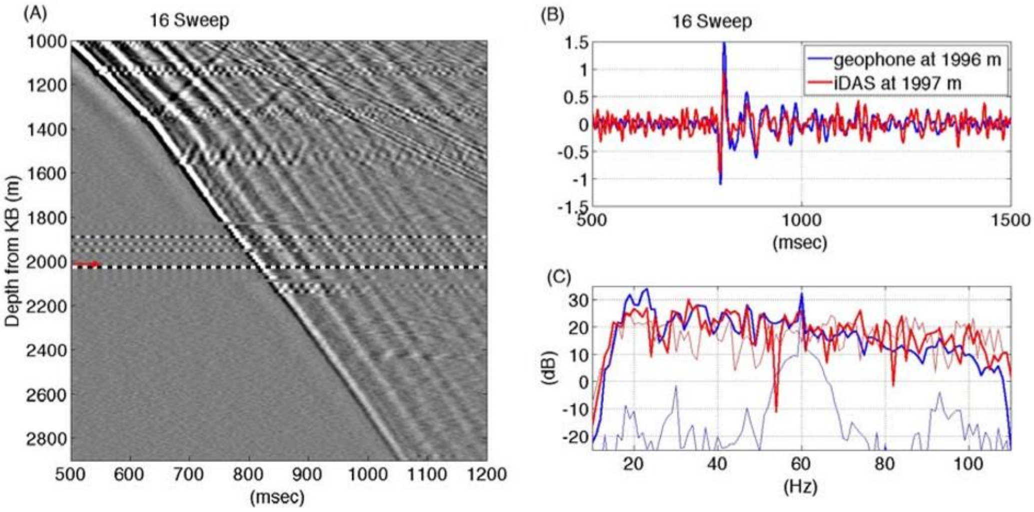

Figure 3.12. Comparison between converted DAS and geophones signals from VSP survey. (Daley et al., 2016).

Figure 3.12 shows the result from a VSP where a deep survey (1000-2800 m) is studied. The soil was loaded at the surface by a vibroseis. The results that is shown in Figure 3.12 is based on 16 tests. The result suggest that a short blow is applied, and that some reflections are visible. At the depth that is considered in Figure 3.12, the wave speed is rather constant. and quite high: about 3500 m/s. The system behaves as a 1-D system with constant velocity. This offers a good opportunity to calculate the particle velocity from the measured strain acc. Eq 3.5. The measured pulse is very short, about 0.05 ms. With the wave speed 3500 m/s the length of this pulse is 175 m.

4 Data acquisition

4.1 Survey site description

The site is localized within Deltares main Campus in Delft (Figure 4.1). The survey site consists of a rectangular area of around 5.0 m width x 70.0 m long, that is in front of the Delta flume facility of Deltares. The ground conditions consist of very soft clay and fine sandy soil, and with a rather shallow water table.

This work has been done as part of the Deltares project 1120377-002 in December 2019:

a)

b)

Figure 4.1 a) Deltares facilities in Delft, and b) test site location parallel to internal pavement road.

Nearby the site, there are low and high frequency noise sources that can potentially affect the quality of the collected acoustic signals. Alongside the test site there is a small pavement road with cars passing by at irregular intervals Figure 4.1 b). Furthermore, the *Rotterdamseweg* street, a usually busy road, is at 160 meters from the test site constitutes the main source of man-made noise in the area.

4.2 Field set-up

The acquisition set-up is displayed in Figure 4.2. The survey lay out is comprised by a 701 - meters fibre optic cable (first 541 meters is a single mode and 160 meters of helical cable) and a set of 7 multi-component accelerometers. The fiber optics line is placed along 60 meters segment and the accelerometers are placed along the first 35 m (5 meters of spacing). Accelerometer numbers 2, 4, and 6 are measuring at y-z direction, and accelerometer numbers 1,3,5, and 7 are measuring at x-y-z components. Below the accelerometers, there are 3 vertical and 4 horizontal fibre optics loops of 30 cms. At positions 1,3,5, and 7 additional single mode fibre optic horizonal loops of 3 m - diameter were placed. All Fibre optic coiled, and straight segments were placed within and on top of a trench of about 60 m length of 40 cm x 30 cm that was partially filled with a sand. Also, 3 – meters diameter shallow holes where dug at accelerometers 1,3,5, and 7 to place the 3-meters loop cable. The trench was partially filled with sand to improve the coupling of the cable with the ground. Note that all accelerometers were placed within the sand layer deep enough to get a good coupling with the ground. The 10 shots positions (the same for both vertical impactor and sledge-hammer impacts) are placed at 3.5 m off the line. Shot positions 1 to 8 are placed right in front the accelerometers, while positions 9 and 10 are placed at 20 and 30 meters from accelerometer 7.

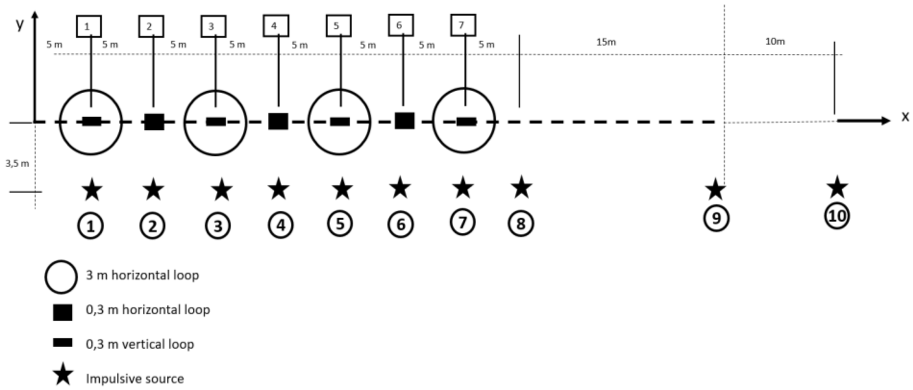

Figure 4.2. Field geometry for data acquisition including accelerometers and source positions. Discontinue line, circular shape, and dark rectangle and square shapes represent spaces where the fiber optics straight and coiled segments will be placed. Impulsive source positions were the same for vertical impactor and sledgehammer.

For convenience, the fibre optics segments (according to length interval) are labelled using the abbreviations (segments ID) as described in Table 4-1. For these measurements we use a standard single mode fiber optic cable (yellow cable) which is sensitive along the longitudinal direction only, and a helical cable (blue cable) that enables sensitivity at both, the longitudinal and perpendicular directions.

Deltares

Table 4-1. Segment description of Fibre Optic Line.

Fibre segment	Length Interval (m)	Segment ID	Description
01	17 - 104	HCL	Horizontal Coiled cable of 3 m diameter Large
02	114 - 216	VC	Vertical Coiled cable of 30 cm
03	226 - 299	HCS	Horizontal Coiled cable of 30 cm Small
04	300 - 348	SSLOG	Straight Section Loose on grass
05	351 - 408	SST	Straight Section in the Tube
06	414 - 472	SSTS	Straight Section on Top of Sand
07	477 - 535	SSBS	Straight Section Buried in Sand
08	570 - 628	SSXBS	Helical Cable Buried in Sand
09	643 - 701	SSXTS	Helical Cable on Top of Sand

One of the straight fiber optic segments was placed inside a plastic tube, so the real conditions of the telecommunication fiber optic cables usually installed inside a tube can be approximated (Figure 4.3a). All fibre optic segments are placed within and on top of a trench of about 60 m length of 40 cm width and 30 cm depth, that is afterwards filled with sand.

Figure 4.3. Fibre Optic line for a) straight sections inside a plastic tube, b) 30 cm diameter vertical loop, c) 30 cm diameter horizontal loop and d) 3 m diameter loop. Yellow cable is the single mode fiber optic cable and the Blue cable is the helical multimode fiber optic cable. All loops were made using 15 m of cable.

4.3 Description of acquisition system

4.3.1 Intelligent Distributed acoustic sensing

The DAS system utilized, is the iDAS (intelligent Distributed Acoustic Sensor), provided by Silixa (https://silixa.com/). Figure 4.4 shows the schematics of iDAS operation where the acoustic field interacts with the backscattered light generated along a continuous fibre optic cable. By analysing the backscattered light and measuring the time between the laser pulse being launched and the signal being received, the iDAS can measure the acoustic signal at all points along the fibre. The length of the cable, the duration of the pulse, the speed of light and data-transfer rate pose a limit to the sampling frequency of the recorded signal.

The iDAS natively measures the rate of change of strain in the fibre or strain rate. The measured strain-rate is an average over a length of fibre equal to the gauge length of the system, which is set equal to 10 m (considered the optimum value to preserve adequate resolution and signal-to-noise ratio). This means that the light that is backscattered over a cable length of 10 m is averaged into one data point. For this experiment, the channel spacing, or spatial resolution utilized is of 1.0 m.

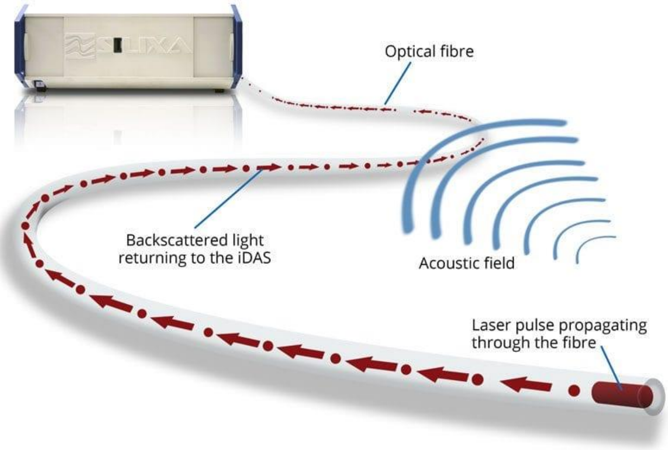

Figure 4.4. Visualisation of the iDAS technique (source: Silixa).

The DAS output can be converted to strain – rate ($\dot{\varepsilon}_{DAS}$) when multiplying the DAS values extracted from the instrument by a scaling factor of 116 nm/sec and the sampling frequency in Hz and divided by the known gauge length Eq. ***4-1***. The strain-rate values are converted to strain (ε_{DAS} in nanostrain) by integrating respect to time and dividing by sampling frequency in Hz (Eq. ***4-2***).

$$\dot{\varepsilon}_{DAS} = \frac{116\text{nm}}{\text{sec}} * \frac{sampling\ frequency\ [Hz]}{gauge\ length\ [m]} \qquad \text{Eq. 4-1}$$

$$\varepsilon_{DAS} = \frac{time\ integrated\ \dot{\varepsilon}_{DAS}}{Frequency\ (Hz)} \qquad \text{Eq. 4-2}$$

4.3.2 Acoustic bandwidth and dynamic range

iDAS has demonstrated to measure frequencies between 0.008Hz up to 100 kHz (for a fibre optic cable of 1000 m length), and a dynamic range of 120 dB (e.g. higher than a short period seismograph) for low frequency acoustic energy with a strain sensitivity down to 5 nanoseconds (Parker, Shatalin, & Farhadiroushan, 2014).

4.3.3 Spatial resolution and measuring range

The iDAS allows a spatial resolution of between 1 m to 10 m, with a sampling resolution to as fine as 25 cm possible, which usually imposes technical challenges (Parker et al., 2014). There is usually a quadratic trade-off between the signal-to-noise ratio (SNR) and the spatial resolution, dz that is $SNR\ \alpha\ (dz)^2$. Thus, iDAS can recover information up to 40 km with an optical loss along the fibre of around 1550 nm, that secures a good SNR. Measurements using longer cable length up to 80 km can be achieved if utilizing amplifiers. Therefore, it has been reported that iDAS is capable of sampling 40 km with 1 m spatial sampling and 80 km with 2 m spatial sampling.

4.4 Field data acquisition

The data acquisition for both, DAS and accelerometers, was carried using independent acquisition systems. Thus, in order to make the same shots collected from both systems comparable, it is required to perform the data collection in synchronized manner, so each record with the same name reference (position, and record number per system), really corresponds to the same shot sequence (each record contains 2 shots for IMPACTOR and 4 shots for SHV). Considering that both systems cannot be mechanically synchronized (both systems start recording at the same time), the systems were triggered manually (Figure 4.5a) almost at the same time. Thus, a proper synchronization should allow multiple shots within the same record, at both DAS and acceleration, appear at the time position.

a)

b)

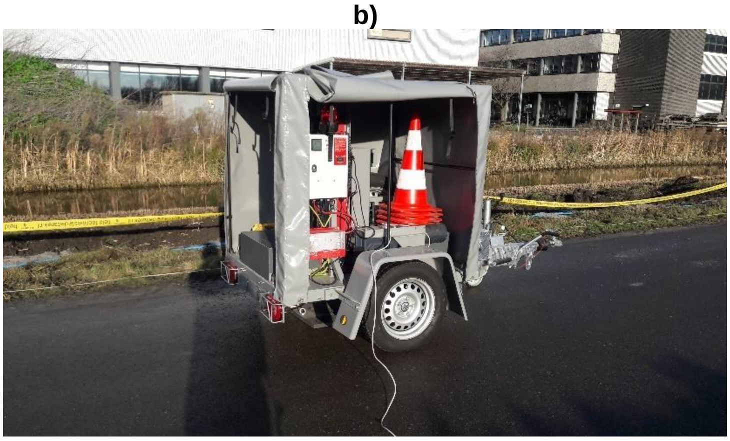

Figure 4.5. a) Data acquisition systems for both DAS and accelerometers, and b) vertical impactor.

Note that due to practical reasons, impulsive source positions were placed parallel and 3.5 m off from the survey line on top of the paved surface (as described in Figure 4.2).

4.4.1 Acquisition parameters

The data collection using both, accelerometers and iDAS is performed simultaneously following the acquisition set-up displayed in Figure 4.3. The acquisition parameters are summarized in Table 4-2.

Although the records were collected almost simultaneously, the lack a proper synchronization requires an additional pre-processing to remove (manually) the remaining time-shift values between accelerometer and DAS traces. All data were collected using a sampling frequency of 1000 Hz. The data was collected in a full day of measurements.

Table 4-2 Collected records as a function of source type

Source type	Source type ID	Number of shots positions	Number of records	Record duration (sec)	Shots per record
Impactor	**IMPT**	10	40	20	2
Sledgehammer Horizontal	**SHH**	7	28	20	4
Sledgehammer vertical	**SHV**	10	3	20	4
Road Bump	**RB**	3	3	180	3
Ambient Noise	AMN	-	2	1800	-

The accelerometers that consist of multi-component transducers, were placed together with the fibre optic line aimed at collecting simultaneous records from all considered sources and with the x-component parallel to the straight fiber optics line. The calibration factors for two and three-component transducers are described in (Table 4-3).

Note that the straight fiber optic segments (SST, SSTS, SSBS, SSXBS, SSXTA from Table 4-1) can be compared with x – component only, because fiber optics is sensible along the longitudinal direction.

Table 4-3 Calibration factor for accelerometer channels

Acceleration component			Fibre Optics component		
Acc_x (mg/volts)	**Acc_y (mg/volts)**	**Acc_z (mg/volts)**	**HCL**	**VC**	**HCS**
-91.806	-96.432	-96.043	x	x	
-205.698	--	-204.625			x
-92.132	-92.945	-89.25	x	x	
-194.818	---	-200.702			x
-200.521	-94.612	-92.82	x	x	
-203.562	---	-199.104			x
-200.481	-89.071	-204.562	x	x	

Table 4-3 also present the locations of coiled segments along the accelerometer positions. HCL and VC are placed below accelerometers 1,3,5, and 7; while HCS are below accelerometers 2,4, and 6.

5 Data processing

5.1 Data-base preparation

To data processing, in time and frequency domain, is performed utilizing a tailor-made python module. The module is designed to automatically load and read DAS and accelerometer records based on the folder structure where the data is stored. The DAS and accelerometer file numbering are properly paired, after carefully verification, so the loaded records correspond to the same sequence of shots (every record contains 2 to 4 shots). Pair of records are loaded indexing the record number, fiber optic segment name, and type of source name as input values.

Once a pair of records is loaded, the module performs:

a) The pre-processing that comprises the following tasks: removing time-shift, baseline correction, amplitude scaling, and selection pair of DAS (individual traces or average from coiled segments) and acceleration traces. This is described in Section 5.2.
b) The processing that comprises spectral analysis as function of source and trace number, time-integration, cross-correlation analysis, and dispersion analysis. This is described in Chapters 6 and 7.

An example of a raw DAS record (for the whole 701 m cable length) using the vertical impactor is displayed in Figure 5.1.

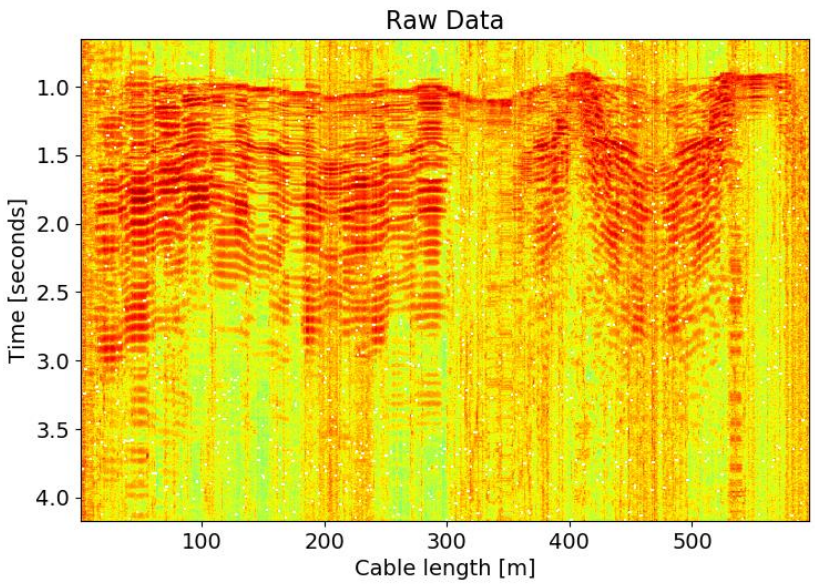

Figure 5.1. Example of a single DAS record with a single shot of the vertical impactor.

5.2 Data pre-processing

Prior to the data processing and analysis, the raw data collected from different acquisition systems and data formats. Thus, before comparing the two datasets it is needed to homogenize the data characteristics in a way that both share the same format, record duration, number of records to be analysed, and a common noise removal scheme.

A description of the pre-processing is presented below:

a) **Data pairing and shift removal:**
The pair of accelerometer and DAS time records are paired (plotted together) and the amount of time-shift is calculated. The time-shift are computed for all records at all shot-positions and for all impulsive sources utilized. The task is developed using the function: *shift_FO_Records.py.*

b) **Baseline correction:**
Raw data from DAS and accelerometers are corrected for zero-offset problems, which causes the vertical axis is off from zero position. Thus, a polynomial 3rd degree function is used to remove the zero – offset problem. This task is performed using the function: *baselinecorr_acc_fo_shotgathers.py*.

c) **Data scaling to strain rate and acceleration**
iDAS raw data are converted to strain – rate utilizing a conversion factor of 11.6 nm/sec. Accelerometer data after baseline correction are scaled utilizing the calibration factor described in Table 4-3. Calibration factors for both DAS and accelerometer records are included in all python functions developed.

d) **Selection of DAS traces**
In order to compare DAS data with nodal accelerometer traces, it is required to select DAS signals that share the same accelerometer coordinates as described in Figure 4.2. For coiled segments the selected DAS trace is computed by averaging 15 traces of fiber optic coiled cable. This task is performed with the following functions:
get_foData_straigth.py
Straight_Aver.py
HorCoil3mloop.py
VerCoil03mloop.py
HorCoil03mloop.py

The selected DAS traces utilizing the python functions are plotted together with acceleration signals (red wiggles of Figure 5.2a) at the same accelerometer positions. Notice that for coiled sections all traces comprising the 3 m diameter (15 traces) are averaged and plotted together with acceleration data collected at positions 1,3,5, and 7 (Figure 5.2b).

a) **b)**

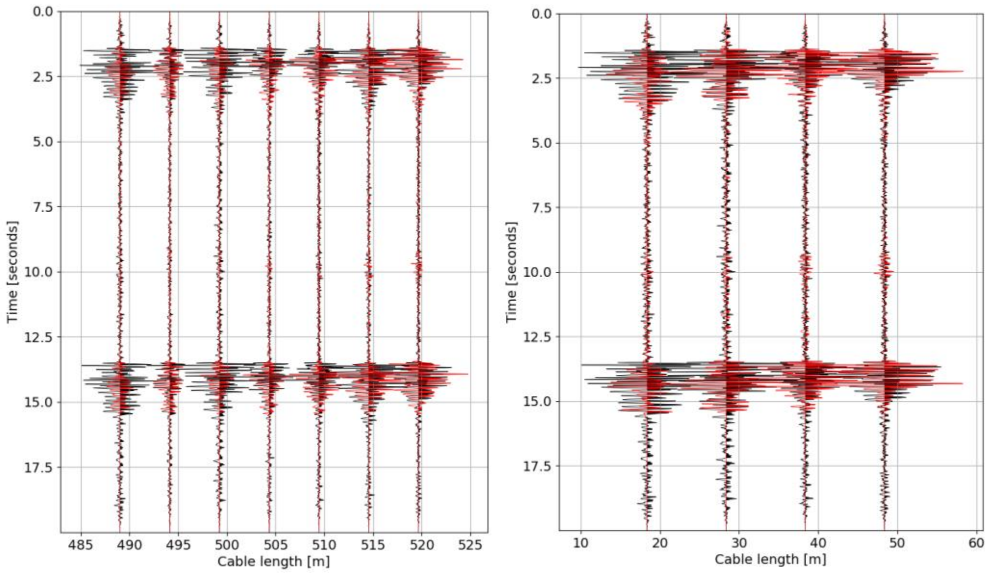

Figure 5.2. Selected pair of traces with the same coordinates for a) straight and b) coiled sections. Signal amplitudes corresponds to strain-rate in strain/sec (DAS – black lines) and acceleration in m/sec2 (accelerometers – red lines).

6 Results for vibration levels

6.1 Frequency domain analysis of DAS and Accelerometer signals

A first assessment of the response of DAS and accelerometers signals is made by calculating the power spectral density functions for the 7 accelerometers and DAS signals for the same coordinates for various source positions. DAS and accelerometers signals are compared using both, the initial accelerations and strain - rate, and the computed strain and velocity. The strain is computed by time integrating the strain-rate utilizing Eq. ***3-3*** as described in section 3.1 For this comparison the analysis if focused on the impactor source.

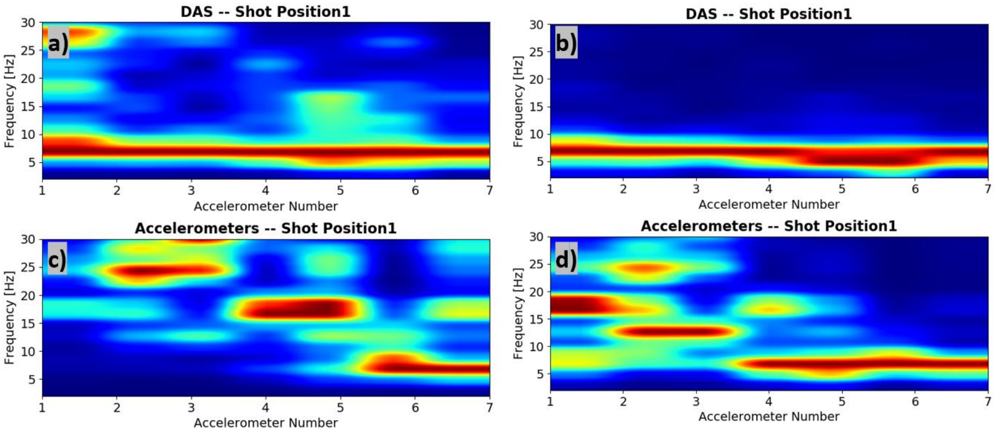

Figure 6.1. Normalized frequency response for both DAS and ACCELEROMETERS utilizing strain-rate and accelerations (a - c); and Strain and velocity (b - d) for source position 1.

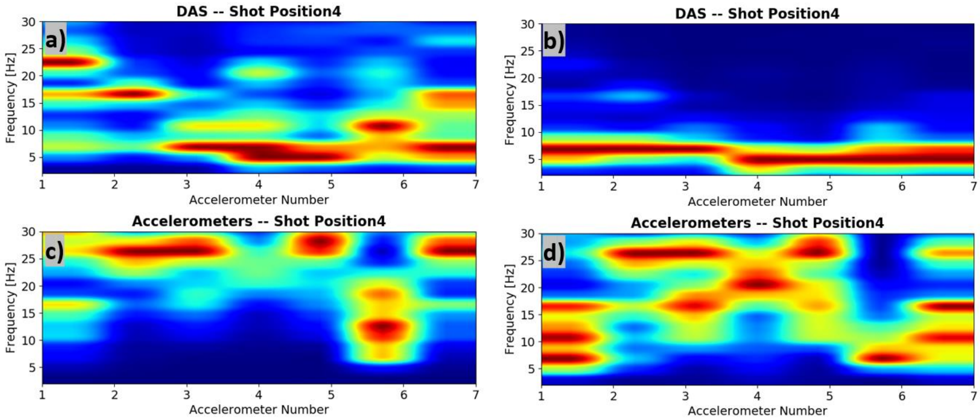

Figure 6.2. Normalized frequency response for both DAS and ACCELEROMETERS utilizing strain-rate and accelerations (a - c); and Strain and velocity (b - d) for source position 4.

Figure 6.1 shows the frequency response for source position 1. It is observed that when using acceleration/strain-rate there is very little similarity between DAS and accelerometers (Figure 6.1a-c). After integrating both signals to compute velocity/strain (Figure 6.1b-d), the frequency response starts to appear similar between frequencies 5 and 10 Hz for the accelerometers 6 and 7, which are the farthest from the source.

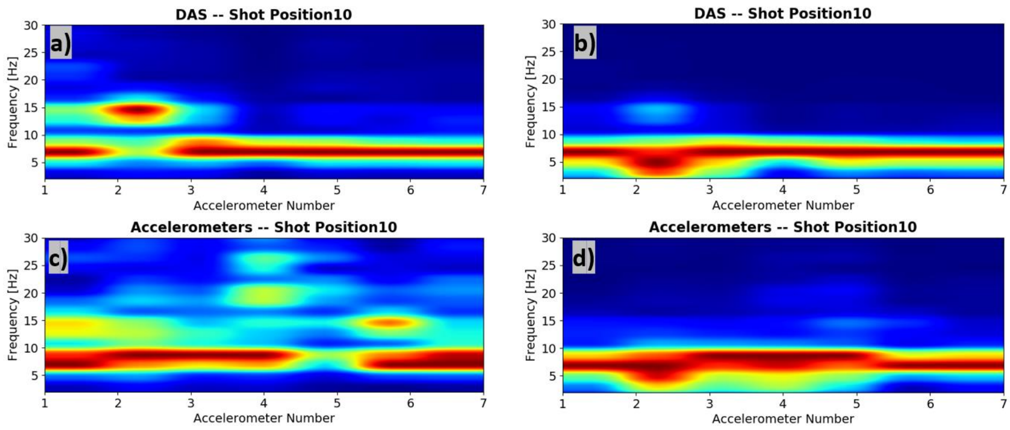

Figure 6.3. Normalized frequency response for both DAS and ACCELEROMETERS utilizing strain-rate and accelerations (a - c); and Strain and velocity (b - d) for source position 10.

At source position 4 (Figure 6.2), the energy pattern with both acceleration/strain-rate (Figure 6.2a-c) appear to be very different from those observed after a source at position 1, but with some similarities at accelerometer positions 1-2 and 6-7 when using the computed velocity/strain signals (Figure 6.2b-d) .Finally, at source position 10 that is at 30 m from the accelerometer line, there is a predominance of low frequency which occurs below 10 Hz. In this case acceleration/strain – rate signals (Figure 6.3a-c) depict very similar energy band, which is better enhanced when using the computed velocity/strain signals (Figure 6.3b-d).

A comparison of the spectral shapes using velocity (Accelerometers) and strain (DAS) of accelerometer numbers 1, 3, 5, and 7 considering the source position 10 is showed in Figure 6.4. It appears that, in general, both, accelerometers and DAS exhibit very similar response with a dominant energy peak between 5 and 10 Hz.

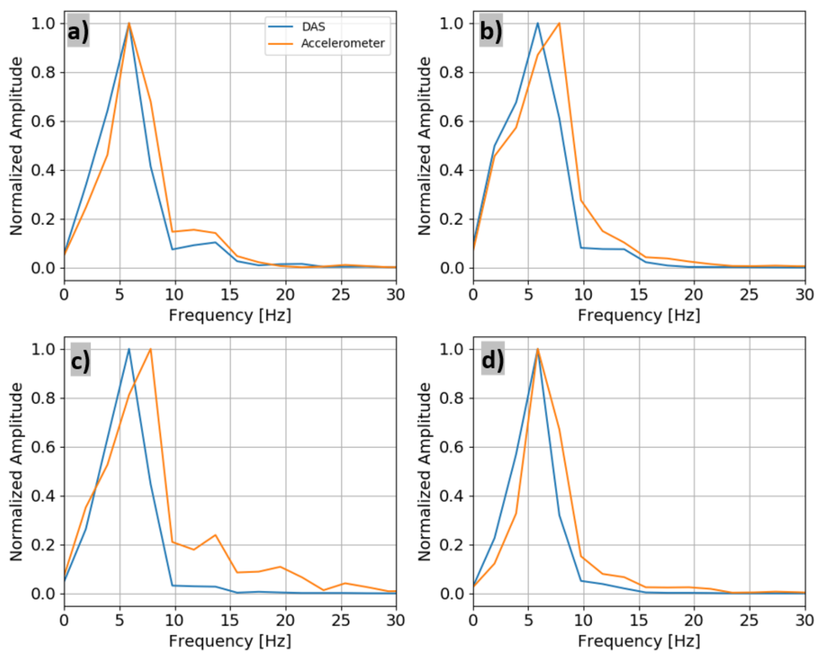

Figure 6.4. Frequency response of accelerometers a numbers: a) 1, b) 3, c)5 and d) 7 for source position 10 using strain (DAS) and velocity (ACCELEROMETER) signals.

Figure 6.5 shows the response of accelerometer number 7 for source positions at 1, 4, 7, and 10. It is observed that the best similarities occur at source positions 1 and 10 which are the farthest distances respect accelerometer number 7.

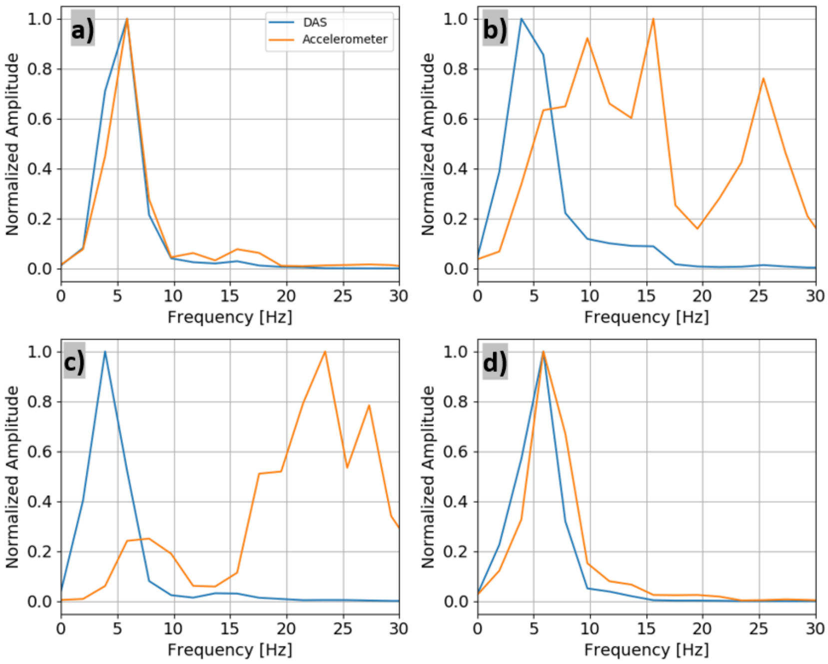

Figure 6.5. Frequency response of accelerometer 7 using source positions a) 1, b) 4, c) 7 and d) 10 using strain (DAS) and velocity (ACCELEROMETER) signals.

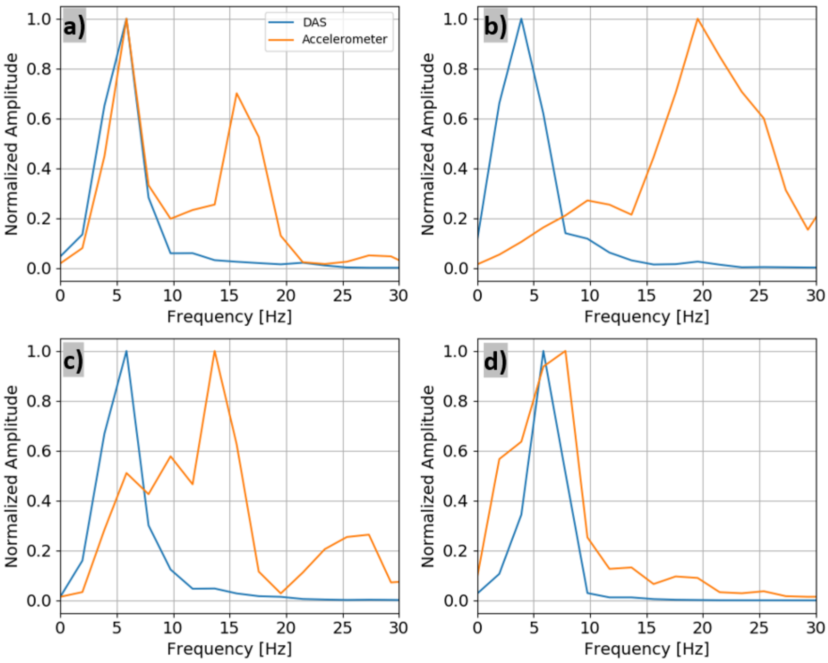

Figure 6.6. Frequency response of accelerometer 4 using source positions a) 1, b) 4, c) 7 and d) 10 using strain (DAS) and velocity (ACCELEROMETER) signals.

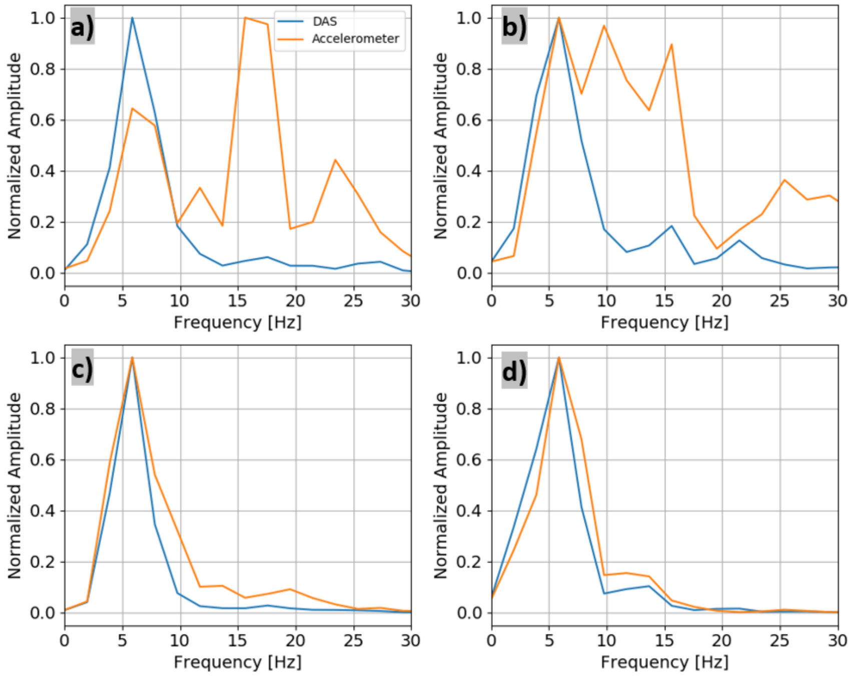

Figure 6.7. Frequency response of accelerometer 1 using source positions a) 1, b) 4, c) 7 and d) 10 using strain (DAS) and velocity (ACCELEROMETER) signals.

The behaviour is observed for accelerometers 4 (Figure 6.6), but more clearly at accelerometer 1 (Figure 6.7) where the increasing source-to-receiver distance also increases the similarities between spectral shapes.

This analysis suggests that the fibre optics leads to signals with the same frequency content in the far field only. In general, the low frequencies propagate further than the high frequencies, as is clearly seen in the accelerometer data. Once a thin frequency band exists in the far field, the similarity is good.

6.2 Time domain analysis of collected DAS and Accelerometer signals

The time domain analysis consists on comparing pairs of DAS and Accelerometer signals. A first analysis consists of computing the signal to noise ratio functions (SNR) for the vertical impactor in Section 6.2.1. The SNR curves allows identifying the specific frequencies where the highest energy occurs, which is used to define specific and common bandpass filter limits for both DAS and accelerometer data.

The similarities between collected waveforms is analysed by means of cross-correlation coefficient. All DAS traces analysed correspond to straight segments of fibre optic cable buried in sand which is the best coupling condition achieved. Only, a brief discussion is made regarding signal strength of coiled segments in Section 6.2.4

Note that one of the objectives is to evaluate whether the averaging along the 10 meters (gauge length) performed during iDAS acquisition, affects somehow, the strenght of signals when using a spatial sampling of 1.0 m. Thus, average @10 m signals and @1 m signals are consistently compared with individual accelerometer signals in Section 6.2.1.

6.2.1 Vertical Impactor source

The strongest source utilized in the survey was the vertical impactor. A first assessment is performed utilizing 7 DAS traces located at the same accelerometer coordinates, referred as @1m DAS data.

The average SNR (spectral ratio between full trace respect to noise segment) function for both DAS and Accelerometer signals (for the 7 accelerometer positions) for source position 10 is displayed in Figure 6.8. It is observed that, for the same loading, the highest energy of accelerometer signals occurs in a wider frequency range compared to DAS. DAS signals appear to be more sensitive at low frequency range compared to accelerometer signals.

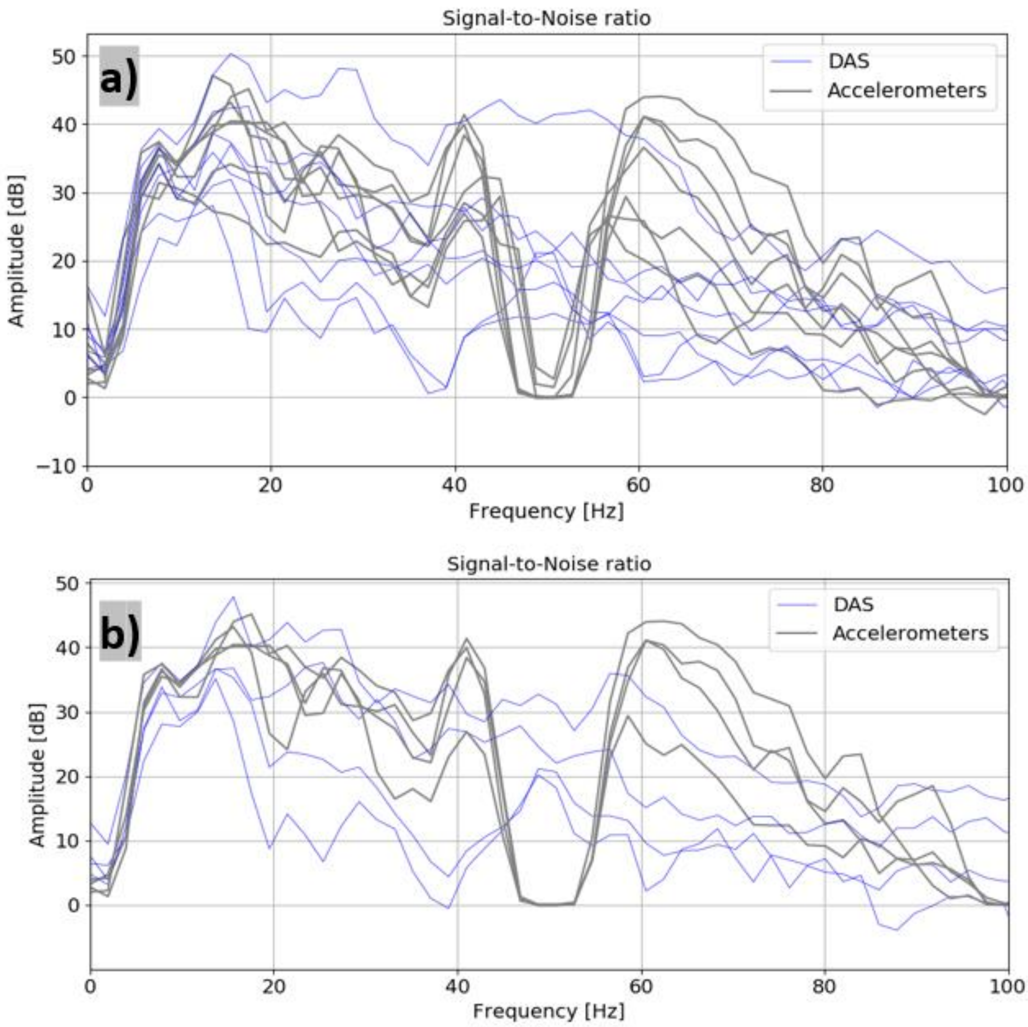

Figure 6.8. Signal-to-noise ratio curves at a) @1m and b) @10m for 7 and 4 receivers respectively.

Both raw DAS and accelerometer traces are normalized and plotted together to analyse waveform similarities of traces collected simultaneously at various receiver positions. Figure 6.9 shows a pair of traces for both @1m and @10m average DAS signals. The raw traces are preliminary filtered [2 Hz to 25 Hz] to enhance the main energy. The similarities between signals is evaluated by computing coherence function. It appears that both pair of signals are reaching the highest coherence in frequency band of 3 Hz - 6 Hz approximately. Notice that the closest the coherence to 1 the more similar the signals are.

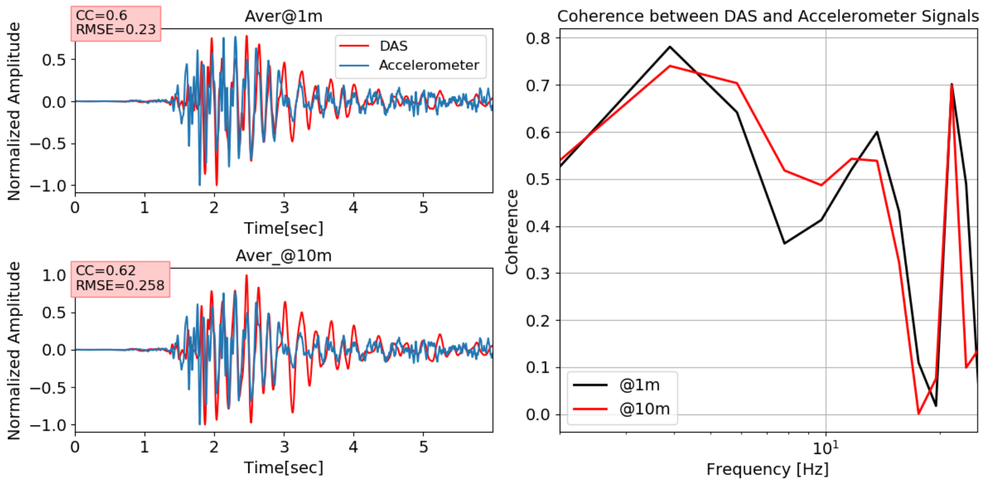

Figure 6.9. Pair of traces for DAS and accelerometer 7 – IMPACTOR.

The same pair of signals is band-pass filtered in the frequency band where the coherence reaches its highest values as depicted in Figure 6.10. Both pair of signals mimic the same number of cycles. Notice that the average @10m traces do not show a significant improvement in the correlation coefficient compared to @1m case.

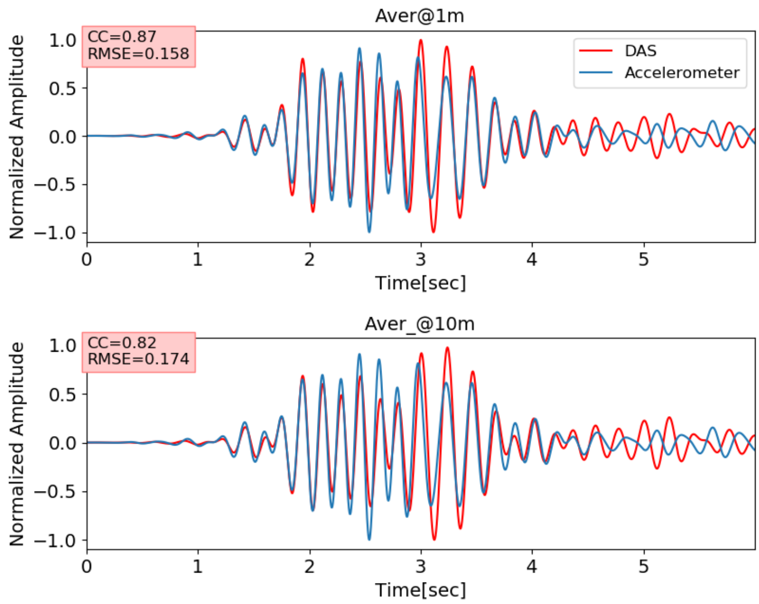

Figure 6.10. Pair of fibre optics and accelerometer traces for @1m and 10@ m average DAS traces for accelerometer 7.

The band-pass filtered waveforms for accelerometers 1, 3, 5, and 7 are plotted together with DAS signals for @1m cases (Figure 6.11). For all cases the cross-correlation coefficient appears between 0.8 and 0.9.

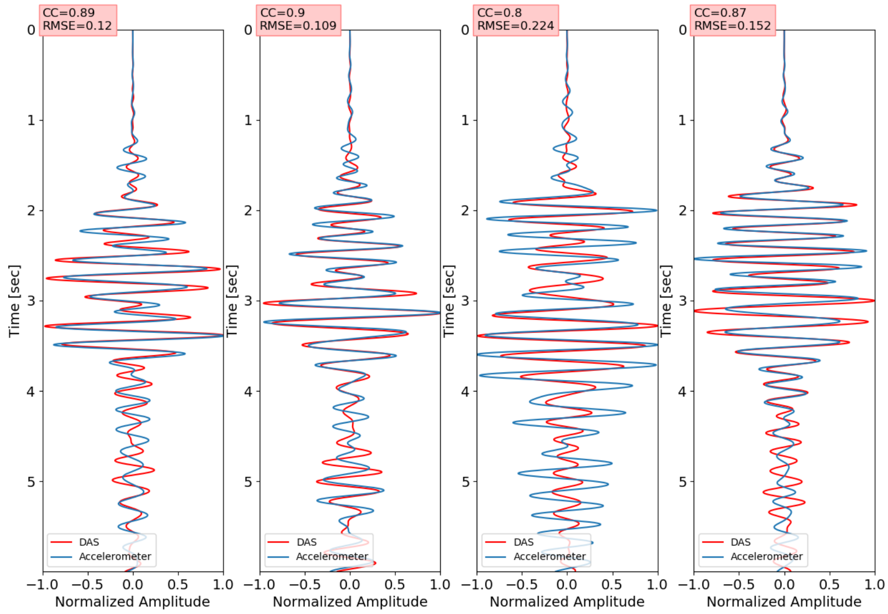

Figure 6.11. Band-pass filtered shotgather [3 – 6 Hz] for accelerometers 1,3,5, and 7 for vertical IMPACTOR source at position 10.

The cross-correlation values for pairs of DAS - accelerometer signals at accelerometer 1,3,5, and 7 is showed in Figure 6.12. In all cases the coefficient is above 0.7. Notice that the @1m traces provided higher coefficient values up to 23% (accelerometer 1) compared to the average @10m DAS signal, while for accelerometers 3, 5, and 7 the average error appears below 2.5%.

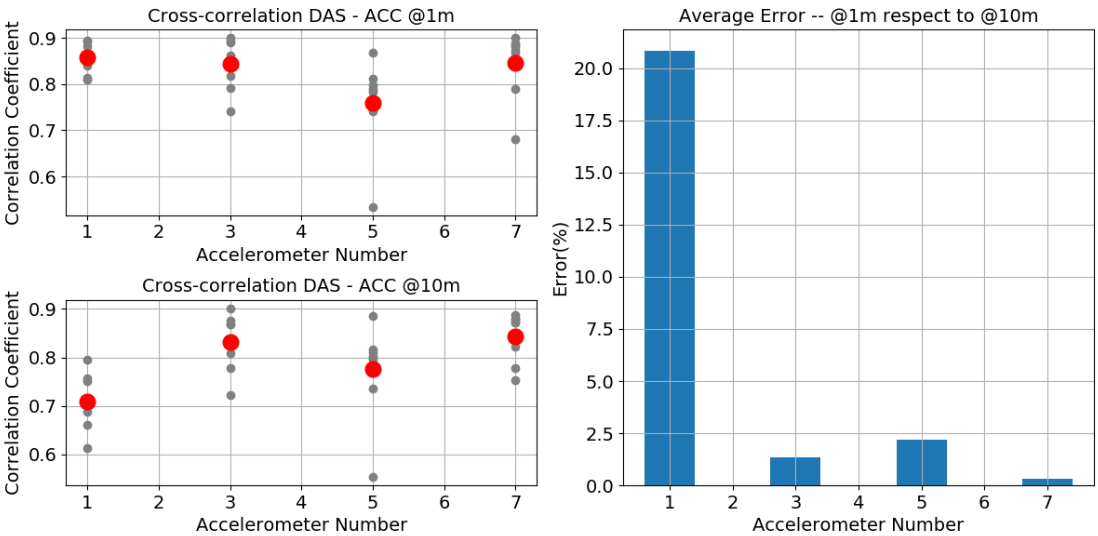

Figure 6.12. Average cross-correlation coefficients (red dots) for DAS signal (@1m and @10m) for accelerometers 1,3,5, and 7. Individual coefficients for 8 individual shots are grey dots.

6.2.2 Sledge-hammer source

A similar analysis is performed using sledgehammer source (SHV) at position 1. The raw data are preliminary band-pass filtered [2 – 25 Hz] to enhance the hammer blow energy. As in the previous case the DAS and accelerometer data are plotted with coherency functions to identify this frequency where both set of data share similar information.

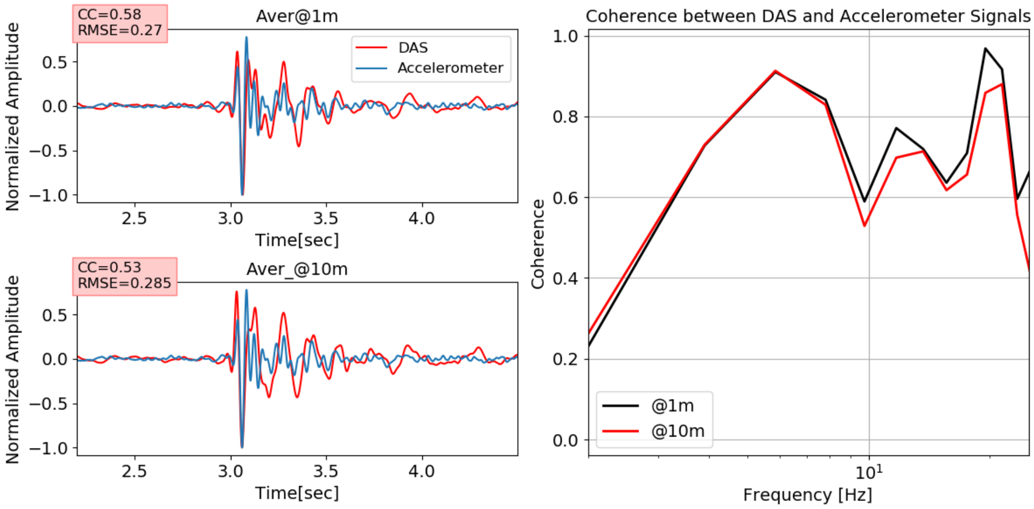

Figure 6.13. Waveforms (left panels) and coherency function (right panel) for pair of traces DAS and accelerometer 3 -- SHV.

There are two frequency bands [5 – 9 Hz and 18 - 24 Hz] where the coherency function is higher than 0.8. Thus, the analysis is performed in both frequency bands.

The resulting waveforms and cross-correlation coefficients are displayed in Figure 6.14. After filtering the signals, both signals appear to be very similar at low and high frequency bands. This similarity, however, does not occur at all traces. In Figure 6.15 accelerometers 1, 5, and 7 depicts very low cross-correlation coefficient indicating almost not similarities between signals, while accelerometer 3 shows a coefficient of 0.8.

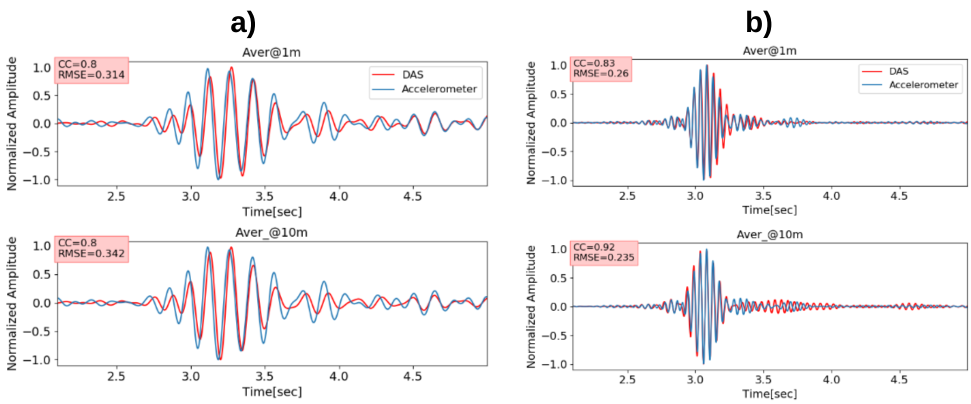

Figure 6.14. Pair of DAS and accelerometer traces for band-filtered traces in a frequency band of a) 5 - 9 Hz and b) 18 – 24 Hz.

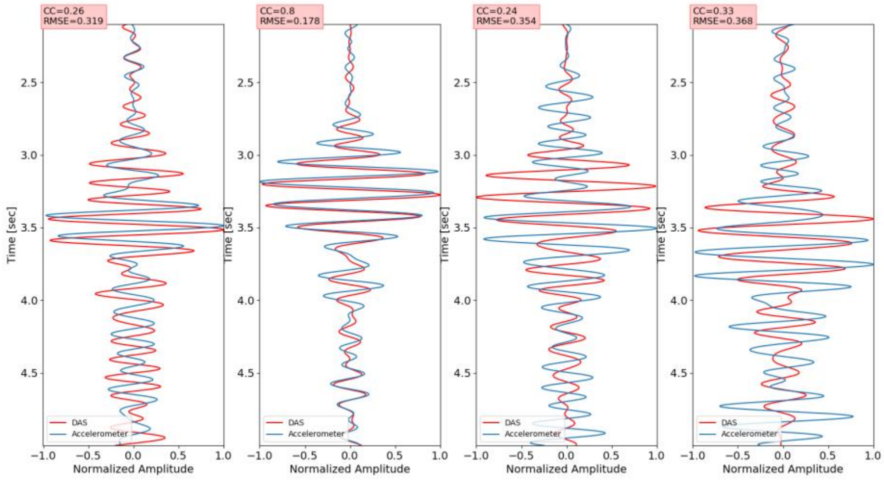

Figure 6.15. Shotgather band-pass filtered [5 – 9 Hz] for accelerometers (left to right) 1,3,5, and 7 for vertical sledgehammer source at position 1.

The same comparison is made for the high frequency band as displayed in Figure 6.16. In this case accelerometers, 1 and 3 depicts rather good coefficient (0.68 and 0.83) while accelerometers 5 and 7 shows lower and negative coefficients.

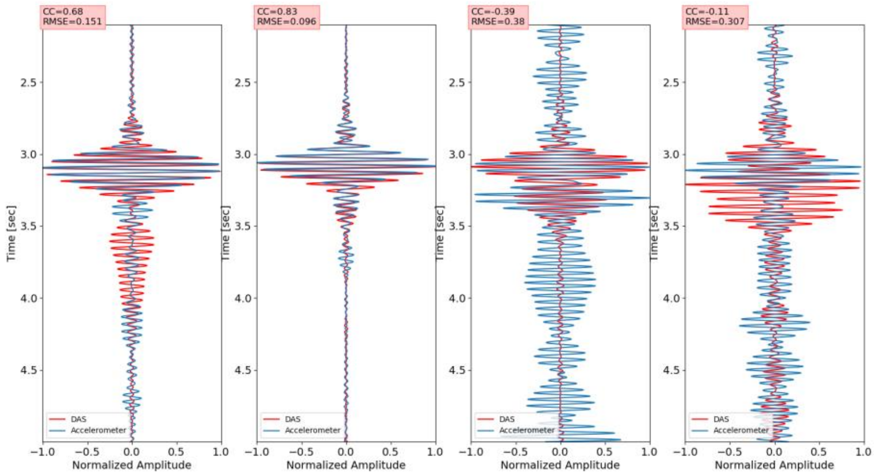

Figure 6.16. Shotgather band-pass filtered [18 – 24 Hz] for accelerometers (left to right) 1,3,5, and 7 for vertical sledgehammer source at position 1.

The cross-correlation coefficients considering multiples shots for both cases are displayed in Figure 6.17. In both cases the highest cross-correlation coefficients are obtained for accelerometer 3. Error bar is not included due to negative correlation values.

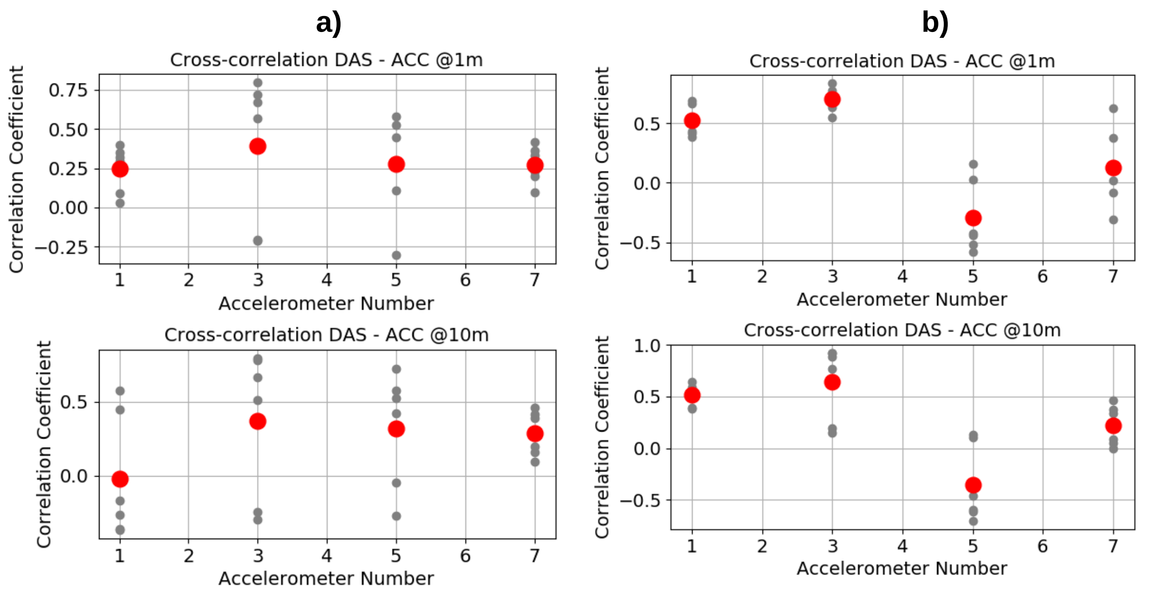

Figure 6.17. Average cross-correlation coefficients (red dots) for DAS signal (@1m and @10m) for accelerometers 1,3,5, and 7. Individual coefficients for 8 individual shots are grey dots. Band-pass filtered a) [5 Hz - 9 Hz] and b) [18 Hz – 24 Hz]

6.2.3 Amplitude attenuation

The attenuation is evaluated by averaging RMS (Root-Mean-Square) of time – domain amplitudes as a function of accelerometer and source positions. The analysis is performed for both IMPACTOR and SHV source types and for positions 7, 9 and 10. All amplitudes are normalized respect to the closest source -to- receiver distance (receiver 7 is 35 meters from the position 10). It is observed that the RMS amplitude for accelerometers do not show the typical amplitude decay respect to the nearest receiver position (Figure 6.18). The attenuation of DAS signals for both @1m and @10m appears to be very similar in all cases.

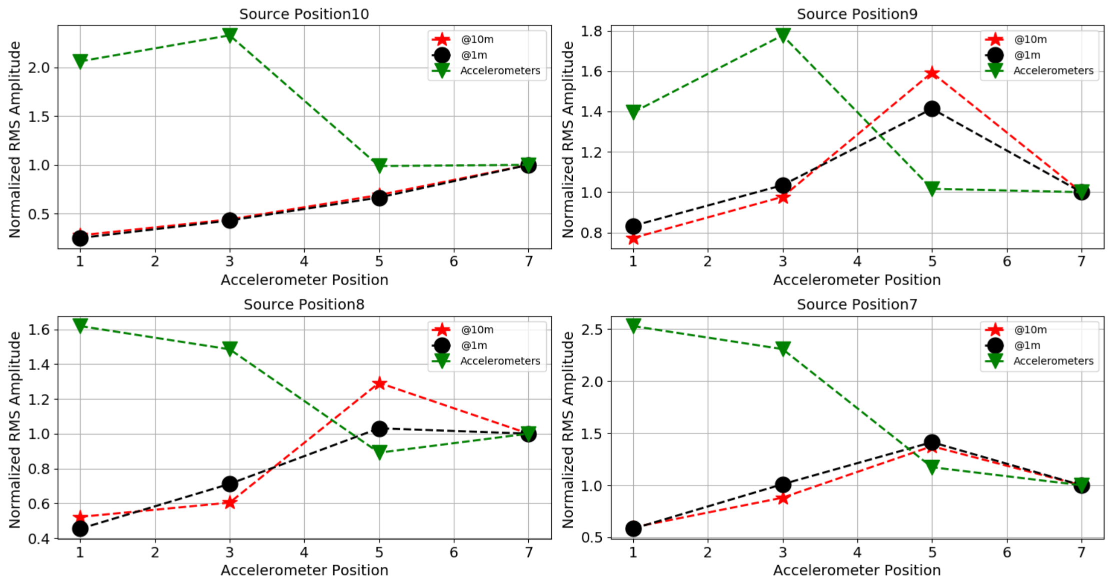

Figure 6.18. Signal amplitudes (RMS) as a function of accelerometer position when using IMPACTOR.

Deltares

A similar analysis is performed for the same source positions but using the sledgehammer source (Figure 6.19). This time the source positions at 7 and 8 shows a decay of amplitude with distance. The source positions 9 and 10 the amplitudes are larger at the farest receivers.

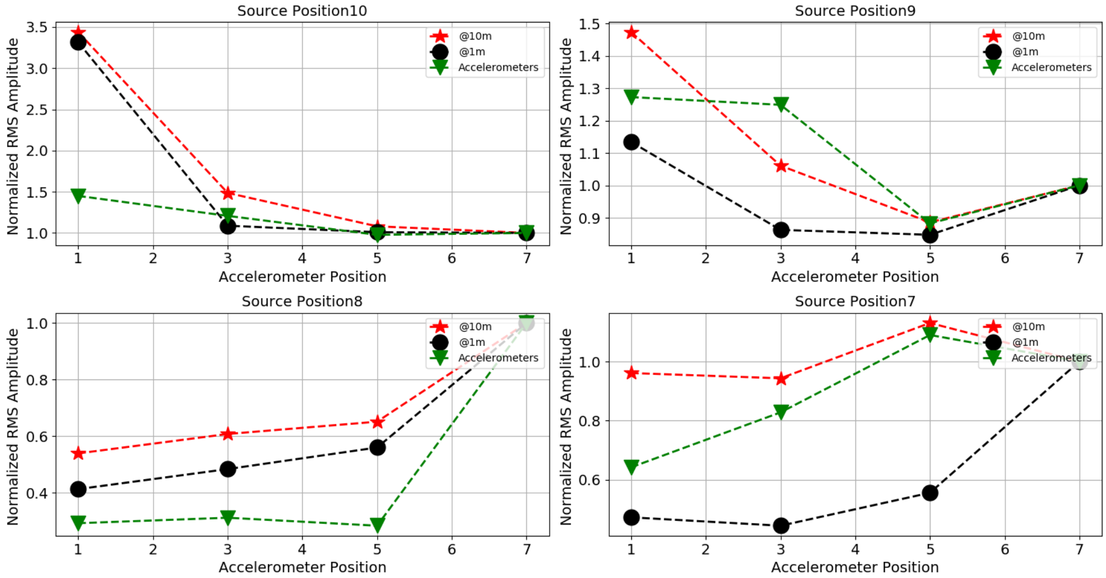

Figure 6.19. Decay functions of amplitudes as a functions of source positions and receiver positions for sledgehammer source SHV type.

6.2.4 Coiled sections

Coiled segments of 3 meters diameter were placed below accelerometers 1,3,5, and 7. The DAS coiled segments were assembled averaging 15-meters of fibre optic cable. As DAS signals were collected at 1 meter of interval along a circular fibre optic cable, not all traces will depict the same waveform due to the differences in the azimuth of the incoming wavefield. In Figure 6.20, only the trace at position 7 shows some similarity (CC=0.68) to accelerometer data.

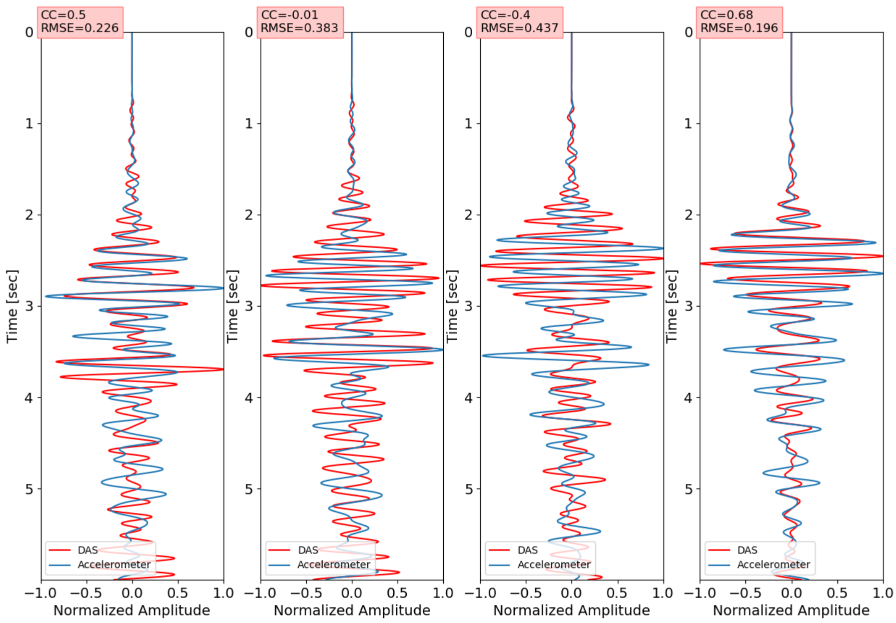

Figure 6.20. Shotgather band-pass filtered [3 – 6 Hz] for DAS and accelerometers 1,3,5, and 7 for vertical IMPACTOR at source position 10.

The traces collected at position 7 are plotted for a singled trace @1m (selected within the 15 m cable segment) and @10m (Figure 6.21). In both cases the cross-correlation coefficients seem to be reasonable high (0.66 and 0.68).

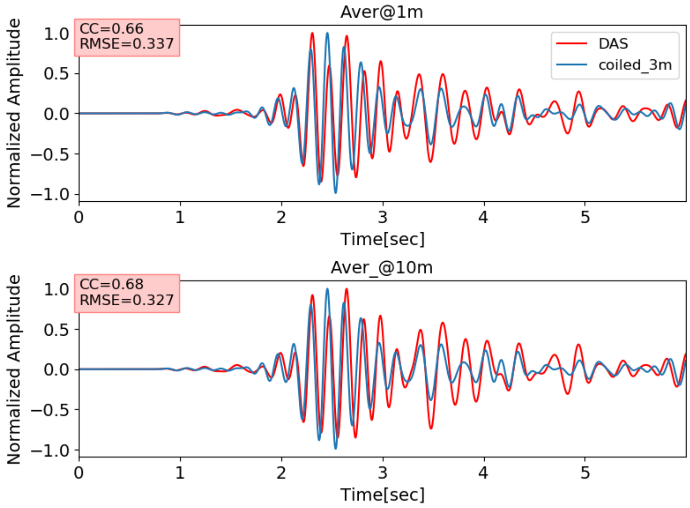

Figure 6.21. Pair of DAS signals for @1m and @1m average respect to average-3 m coiled traces. Accelerometer 7.

A similar comparison is made using the vertical coiled segments (0.3 m of diameter) place below accelerometer 1, 3, 5, and 7. The highest correlation value observed is of 0.86 at accelerometer 1, while the other accelerometers the correlation is below 0.5. Note that the accelerometer component utilized for this comparison is the vertical component.

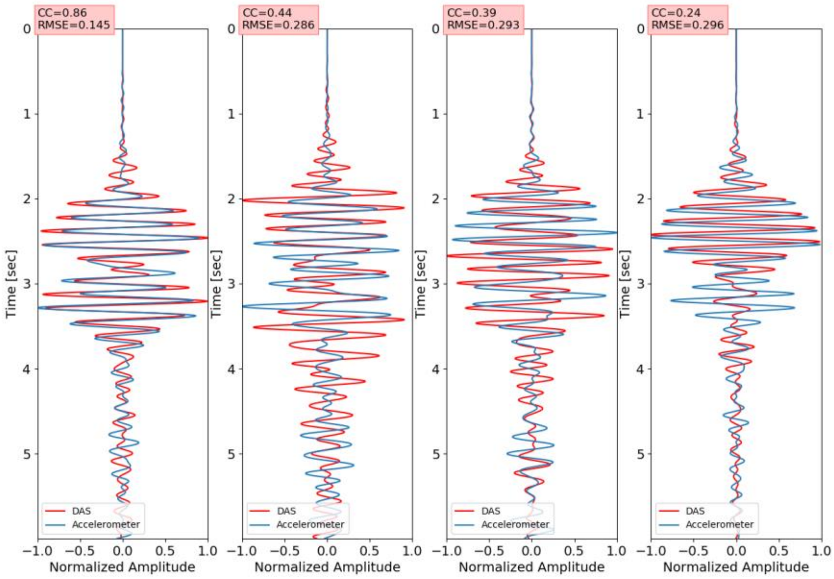

Figure 6.22. 30 cm diameter vertically coiled Fibre optic segments below accelerometers 1, 3, 5, and 7.

6.3 Velocity – to – strain ratio from accelerometers and DAS signals

The strain-rate and acceleration time - histories are converted to strain (nm/m) and velocity (nm/sec) time - histories. If assuming that DAS and accelerometers provides the same particle velocity information, the ratio of the RMS amplitude of velocity to strain, should be interpreted as the apparent phase velocity (c), as described in ***Eq. 3-6***.

Figure 6.23 shows the computed velocity/strain ratio as a function of accelerometer number for both vertical impactor and SHV. In general, for the vertical impactor and SHV sources the velocity/strain ratio values appear to be below 200 m/sec and 100 m/sec respectively. The highest difference appears at accelerometer position 6 that could be caused by coupling issues of the transducer as observed in the PDS spectrograms.

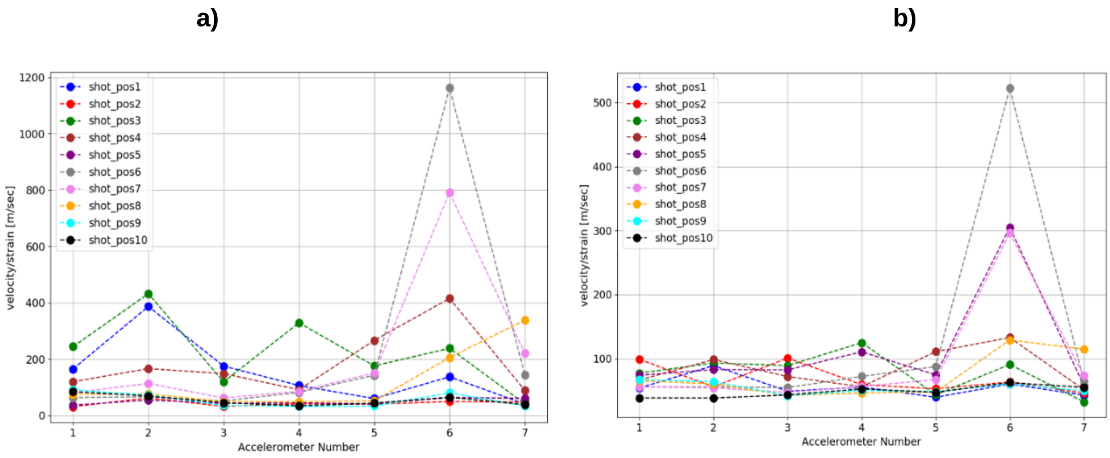

Figure 6.23. Velocity - to - strain ratio for 10 shot positions for a) vertical impactor and b) sledgehammer.

A more detailed analysis is performed is comparison shot positions 9 and 10 for both impactor and SHV source types (Figure 6.24). For impactor source (Figure 6.24a), if we skip accelerometer 6, the velocity/strain ratio shows a consists increment with distance which is consistent with the longer wavelength (propagates at lower frequency) observed with accelerometer 1. On the other hand, when using the sledgehammer source there is reduction of the amplitudes observed at the farest accelerometers, which may be caused by the less amount of energy delivered by the hammer blow compared to the vertical impactor. The insufficient energy causes more attenuation at the farest receivers.

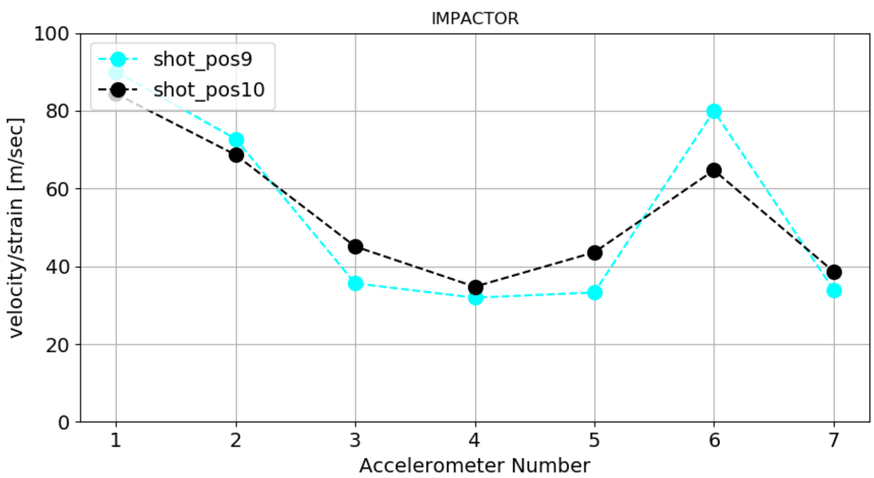

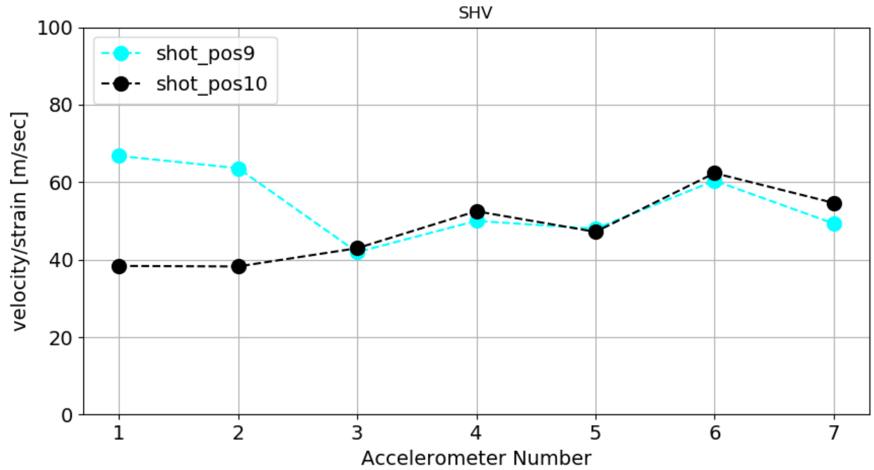

Figure 6.24. *Velocity/strain ration computed at 7 accelerometers positions for both impactor (top) and sledgehammer (bottom) sources considering positions 9 and 10.*

6.4 Effect of coupling conditions for all fibre optic segments

We evaluate the frequency response of straight segments considering various coupling conditions. In Figure 6.25, average Power-Spectral-Density curves are plotted for all cable sections. It is observed that for the case of coiled segments (green curves), depict very similar shape and amplitude, while straight sections the sharp variability in coupling conditions causes a prominent deviation specially in those segments of cable that are not coupled within the sand layer. The effect of coupling conditions specially for straight section is clearly observed when computing the relative error considering the SSBS condition as reference.

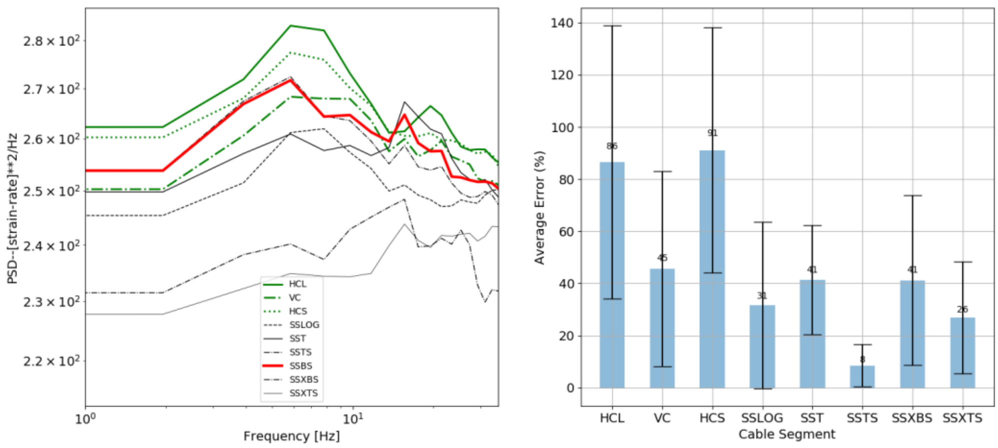

Figure 6.25. *a) average power-spectral density spectrum for all FO sections and b) standard deviation (blue bars are the average) relative to buried cable (SSBS) condition. Coiled sections are in green color. Red line is the one assumed with the best coupling condition.*

The variability of coupling conditions is assessed if computing the relative error for various source positions Figure 6.26. It is observed that error computed from shot positions 1,4, and 7 shows a similar error distribution with the lowest variability at SSTS. Notice that the error computed from shot position 10 deviates a lot from closer shot positions.

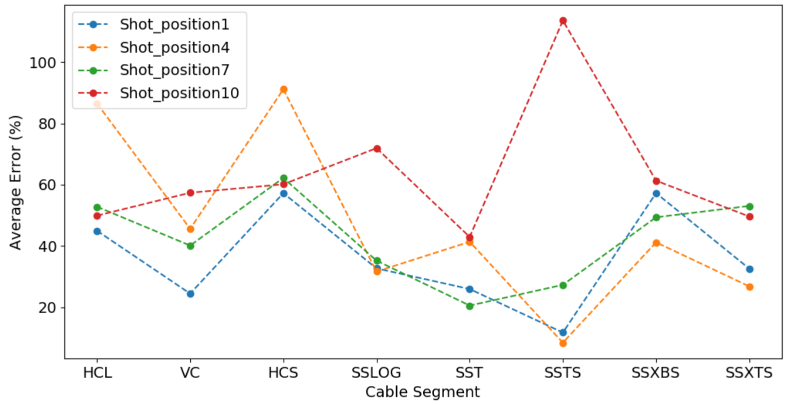

Figure 6.26. Variability of average spectral amplitude as a function of shot position for all fibre segments considered.

Based on these results the coupling condition plays an important role. Average errors in the strain measured by the system from 10% up to >100% are observed. For separate frequency bands the differences might be even higher.

6.5 Equivalent geophone time-history velocity signal

The collected DAS signals are compared to velocity-times history computed from time-integrating collected acceleration records. We evaluate the reliability of the computed equivalent velocity time history by means of Cross-correlation coefficient and ratio of RMS of pair of DAS and time-integrated acceleration data. We focus the analysis in the comparison individual trace (@1m) and average of 10 traces labelled as @10m.

Prior to the integration, the DAS and accelerometer data are scaled using the proper instrument provided (and for the case of DAS the data are converted to strain-rate. Figure 6.27, shows a pair of DAS – Accelerometer traces for a single component along the fibre optic line. The data were band-pass filtered in frequency range between [2 Hz – 8 Hz] to enhance the dominating low frequency energy.

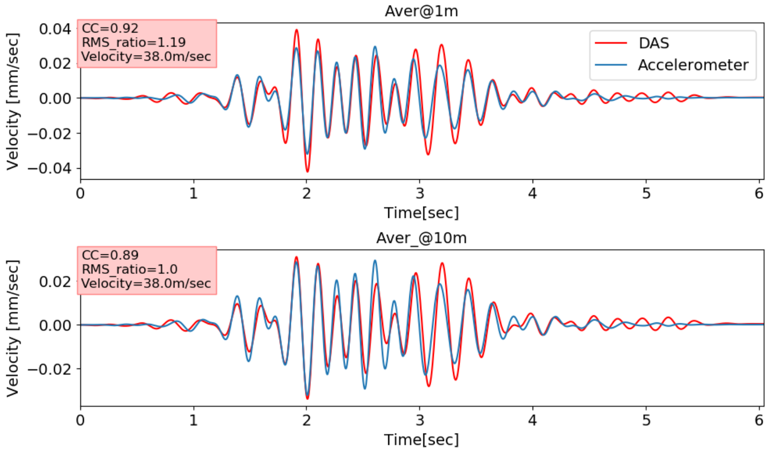

Figure 6.27. Velocity time history for pair of DAS and accelerometer signals considering 1.0 m and 10.0 m DAS average signals (IMPACTOR source at position 10).

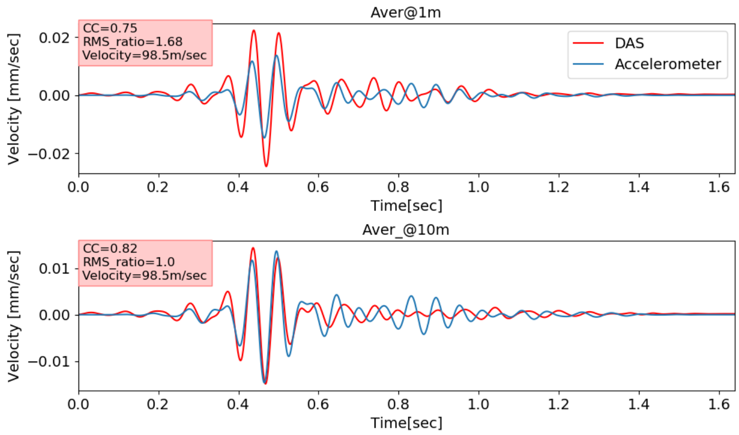

Figure 6.28. Velocity time history for pair of DAS and accelerometer signals considering 1 and 10 m DAS average signals (SHV source at position 1).

For the IMPACTOR source the wave forms share very similar information up to 0.92 (if using a narrower filtering frequency band of 3 Hz - 6 Hz). To search for the appropriate local velocity, the amplitudes are scaled using a range local velocity value until the ratio of RMS reaches 1. In Figure 6.28, a local velocity of 38 m/sec and of 98.5 m/sec for SHV in Figure 6.28, makes the ratio of RMS=1 which should be equivalent to the velocity structure along the fibre optic cable. This procedure can be performed for accelerometers 1,3,5, and 7 when DAS are averaged with @1m and @10 m.

The procedure previously described is implemented for traces 1,3,5, and 7 and for 8 individual IMPACTOR shots for both average cases, @1m and @10 m. As expected, the signals collected in accelerometer 7 seem to share similar information up to a 70% (Figure 6.29). Notice that the accelerometer 7 is the closest to the impactor source, which explains the strongest correlation observed. When comparing both cases, the case of @10m depicts more stable variation compared to @1m case.

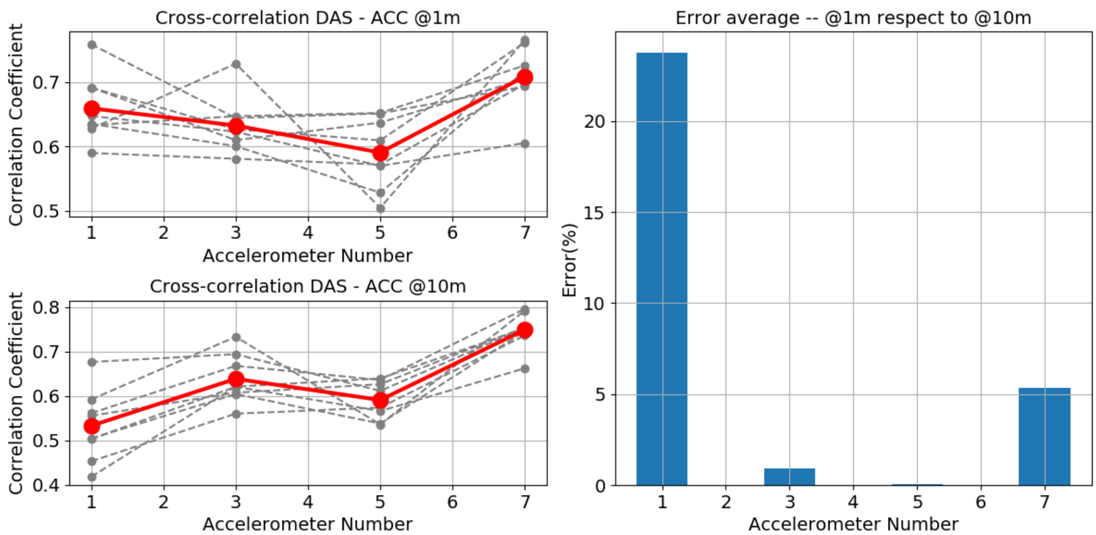

Figure 6.29. Cross-correlation coefficient and error distribution for accelerometers 1,3,5, and 7. All signals band-pass filtered [2 Hz - 8 Hz].

The best local velocity values that provide the same average amplitude (RMS_ratio = 1.0) for the 4 accelerometer positions considered, are displayed in Figure 6.30. The velocity value seems to increase while the source to receiver distance increases. The average velocity seems to vary from within 40 m/sec to 100 m/sec range. For the case of @1m the velocity appears to be less variable providing more stable velocity values. Furthermore, the error between @1m and @10 m case appears below 25%.

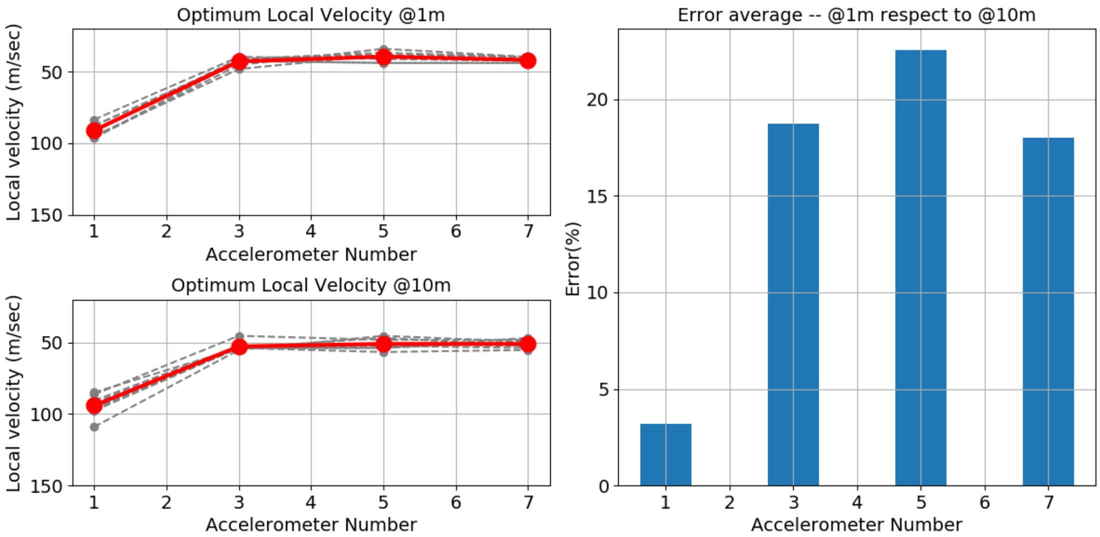

Figure 6.30. Optimum local velocity error distribution for @1m and @10m average velocity for accelerometers 1,3,5, and 7.

The average velocities for @1m and @10m cases are plotted together (
Figure 7.10) with the lower (14 m depth) and upper (2 m depth) boundaries of average velocities (Vp) with depth of the three computed velocity profiles displayed in
Figure 7.9. It is observed that the computed local velocities fall within the limits both for passive and active surveys.

7 Results for surface wave analysis

7.1 Active surface waves

Phase velocity spectrum for all coupling conditions

To account for the whole spread length of 60 m the MASW dispersion images are computed utilizing the source position 10 and the impact source. The shotgather for fibre Optics segments SST, SSTS, SSBS, and SSXBS and its associated dispersion images are displayed in Figure 7.3

a)

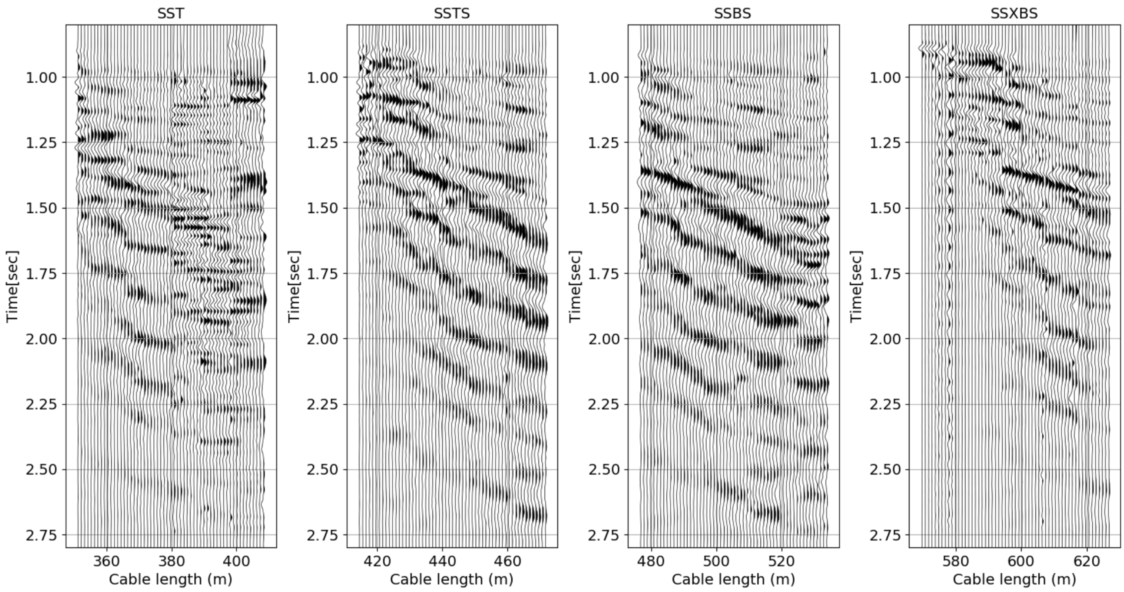

Figure 7.1. Collected shot-gathers from different fibre optics segments: SST, SSTS, SSBS, SSXBS.

The frequency-wave number (F-K) spectrum shows the wave number/phase velocity range where the maximum dispersion energy appears. F-K spectrum is useful to identify potential dispersion energy coming from other sources that not necessarily correspond to the actual hammer blow utilized as active source. Nevertheless, the dispersion analysis for active and passive analysis will be performed in the frequency – phase velocity domain.

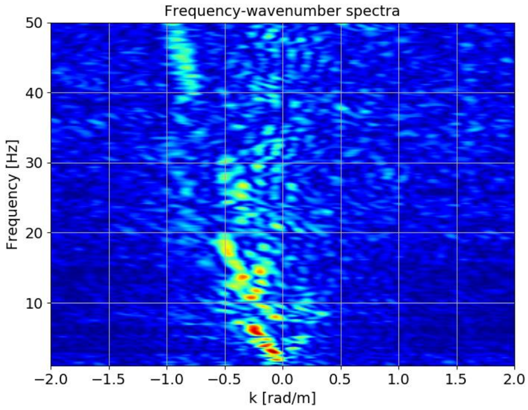

Figure 7.2. Frequency - wave number spectrum for a shotgather collected in SSBS segment.

The phase velocity spectra for 4 straight fibre optic segments is displayed in Figure 7.3. The average DI are obtained from 8 individual shots. To account for geometrical constrains the maximum wavelength considered should not be larger that the survey line that is 57 m. The inverted velocity profiles should not be about more than ¼ the maximum wavelength, so in this case the reliable exploration depth is about 14 m.

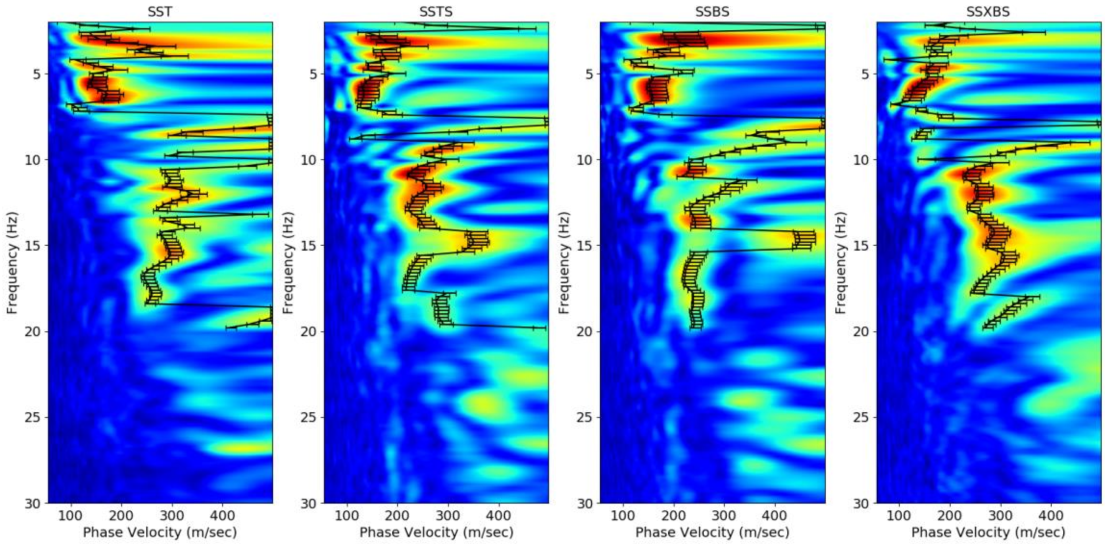

Figure 7.3. average dispersion images for SST, SSTS, SSBS, and SSXBS cases.

Average dispersion curves

The average dispersion images for the 4 coupling conditions considered are utilized to extract the dispersion curves for both fundamental and higher modes. All peak values are displayed in Figure 7.4. It is observed that the fundamental model (2.5 Hz – 7.5 Hz) all cases depicts a similar dispersion trend, while the second mode (7.5 Hz – 16.2 Hz) there is more dispersion energy, especially at frequencies above 12 Hz where all peaks appears to be less similar.

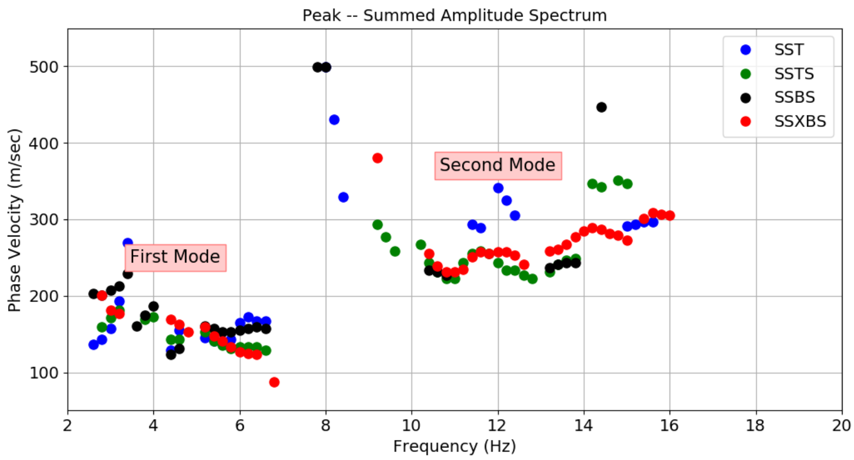

Figure 7.4. Peak energy of dispersion images for SST, SSTS, SSBS, and SSXBS coupling conditions considered.

The variability among coupling conditions is better described using a bar diagram that portraits the average error and standard deviation for both modes, using the SSBS conditions as references. It clearly observed that the fundamental mode the average error varies between 11.2 to 21.4 % while the higher frequency mode varies between 17.56 % up to 29.102 %.

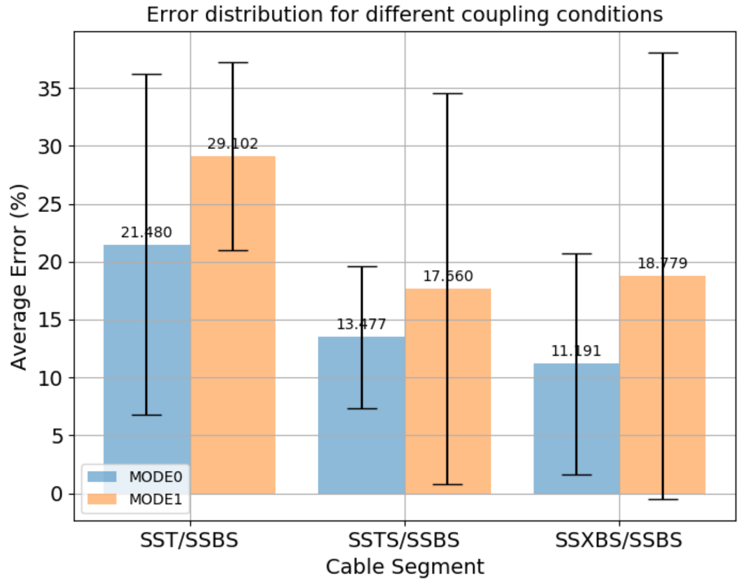

Figure 7.5. Average Error in percent for coupling conditions SST, SSTS, and SXBS respect to SSBS.

7.2 Passive surface waves

Ambient Noise

Ambient noise records were collected during 1 continuous hour. The collected records are utilized to compute active-like records or virtual shot-gathers using SST, SSTS, SSBS and SSXBS segments. The collected records are based-line corrected and band-pass filtered [2 Hz to 30 Hz]. Figure 7.6 shows the computed virtual shot-gathers. Clearly, the SSBS shows a coherent waveform pattern, while in the other cases no coherent waveform slopes are observed.

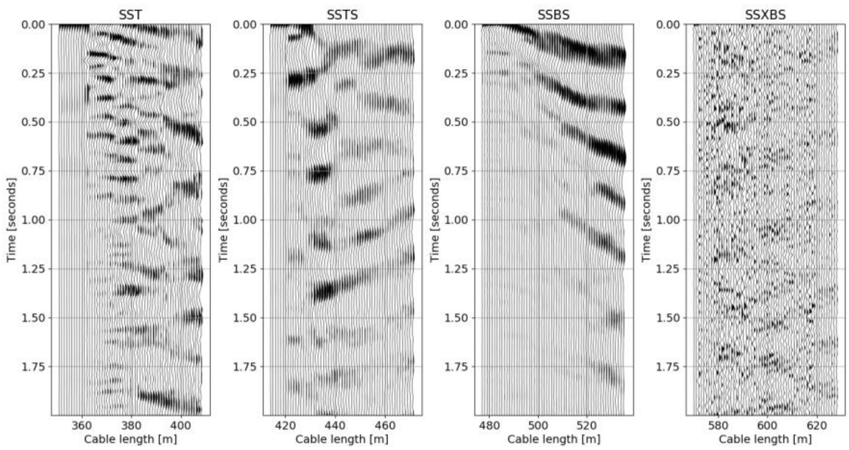

Figure 7.6. Computed shotgather from cross-correlation of ambient noise.

The phase velocity spectrum (dispersion images) for all computed virtual shot-gathers are showed in Figure 7.7.

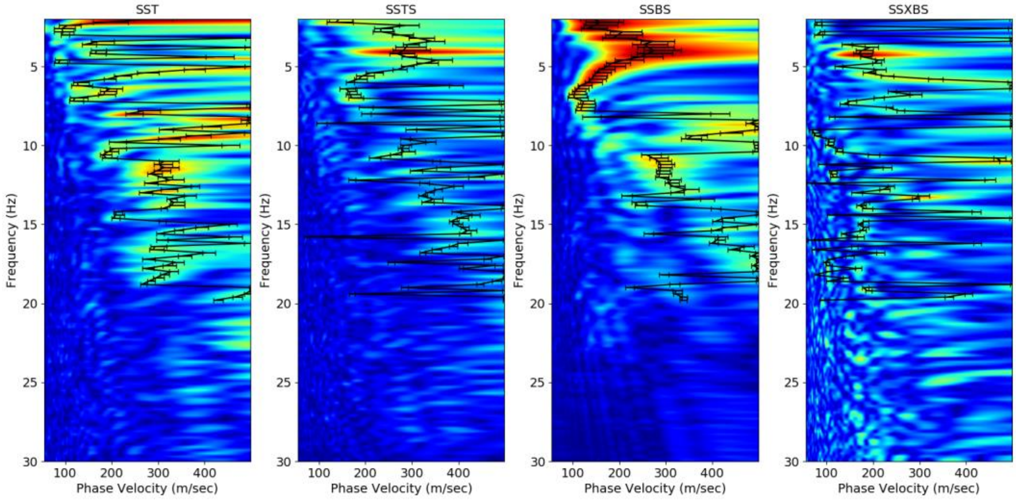

Figure 7.7. Dispersion images for all coupling conditions considered.

Finally, the computed phase velocity spectrum for both active and passive survey are displayed in Figure 7.8. Both images are plotted together with the combined dispersion image from both active and passive.

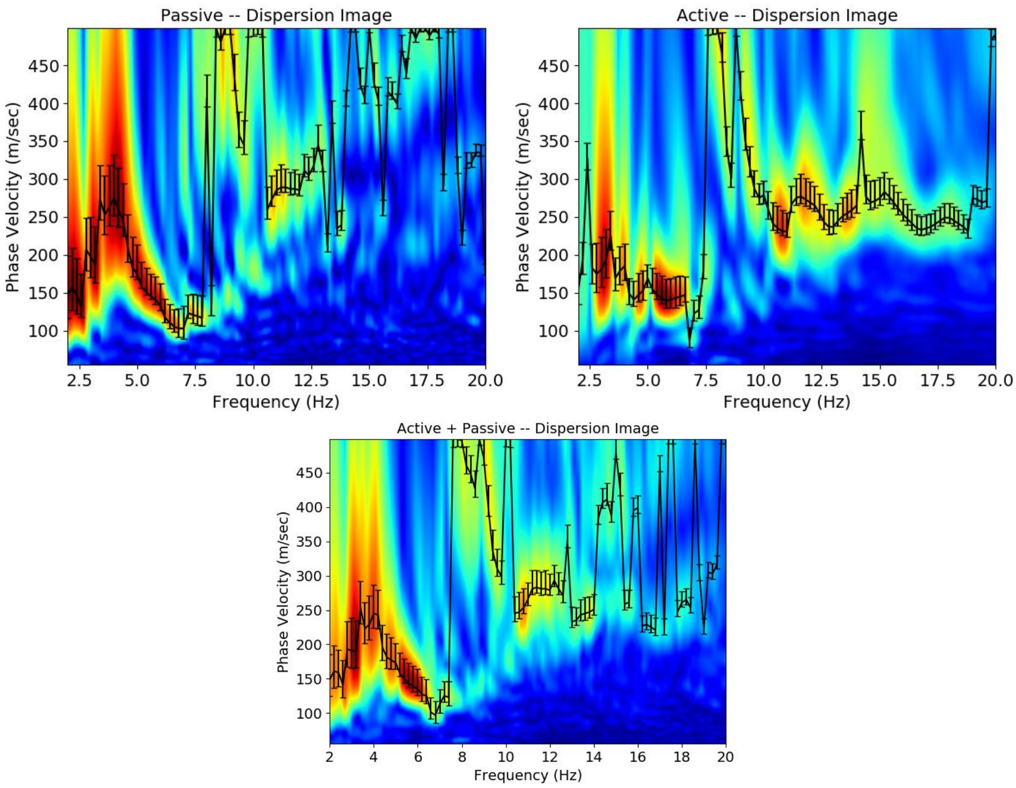

Figure 7.8. Computed dispersion image for SBSS segments for active, passive, and active + passive surveys, including uncertainties of peak energy.

7.3 Velocity structure at the test site

The P-wave velocity structure is proportional to the longitudinal direction of the fibre optic line that can be used to convert the DAS strain signal to equivalent geophone velocity time history signal. P-wave velocity with some knowledge of the Poisson’s ratio can be estimated using S-

wave velocity obtained from dispersion analysis. The S-wave velocity structure is computed for all dispersion cases determined
Figure 7.9. The analysis is performed utilizing all computed dispersion curves active, passive and active+passive.

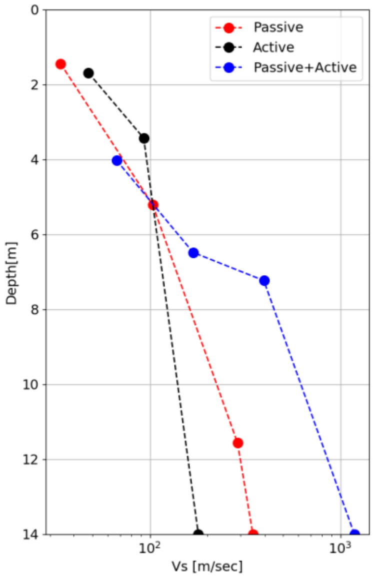

Figure 7.9. Inverted dispersion curves and velocity S-wave profiles for a) Passive (misfit=0.44), b) Active (misfit=1.99) and c) Passive + Active (misfit=0.63) surveys.

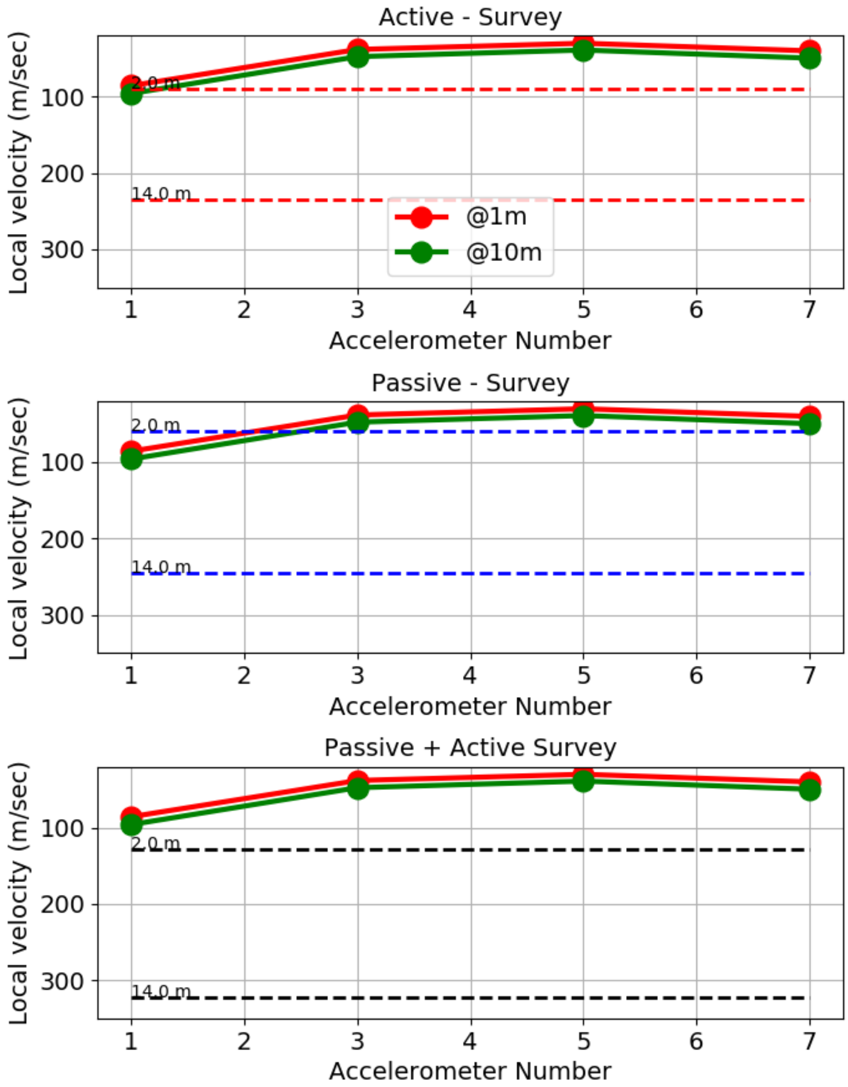

Figure 7.10. *Relation between computed optimum Vp local velocity and average Vp velocity profile (2.0 - to -14.0 m as reference depths) considering active, passive and active + passive. Vp are obtained by converting Vs to Vp using a Poisson's ratio typical for sandy soils of 0.25.*

8 Discussion

Signals generated using various source types are collected simultaneously using both DAS and accelerometer devices. The time and frequency analysis showed that both DAS and accelerometers retrieved energy in a very similar frequency band for both sledgehammer and vertical impactor. When comparing both accelerometers and DAS waveforms, the unidirectional nature of DAS enabled the comparison only along the longitudinal direction and in a limited frequency range. Initially, the both types of waveforms were compared using strain-rate and acceleration data. For those shot positions close to the accelerometer positions, the frequency response showed almost no similarity because DAS energy consistently appear below 10 Hz, while accelerometers exhibits energy in a higher frequency band [15 Hz - 30 Hz]. On the other hand, the farest shot position (shot position 10) both DAS and accelerometers appears in a very similar frequency band (5 – 10 Hz). The difference in frequency response may be due to that DAS retrieves ground vibrations in similar way as seismometers (velocity units), while accelerometers provide the actual acceleration time-history induced to the ground. Thus, a more realistic comparison may be carried out converting the accelerometer output into velocity which is achieved in frequency domain e.g. if multiplying by the inverse of the circular frequency ($1/\omega$).

The basic formulation of particle velocity computed from DAS signals requires converting strain-rate to strain [nm/m], so for consistency the accelerometer signals are converted to velocity [nm/sec]. Therefore, the comparing the frequency response of both strain and velocity time-histories, both spectral shapes appear more similar characterized by a prominent energy peak in a very similar frequency range, for all shot positions. The coupling effect was analysed in frequency domain by computing the power-spectral density functions of all Fibre Optics segments. The coiled segments depicted very similar spectral shape but with some differences in amplitude which could be explained by the variable geometries and coupling conditions. Likewise, the effect of various coupling conditions is observed in the amplitude and shape of the PDS curves. The variability of the average energy of straight segment is computed using SSBS as the reference. The coupling conditions seems to play an important role to properly capture the source energy. Clearly, the SSTS depicted a very similar spectral shape compared to SSBS, while SSXBS despite of being buried did not capture the same spectral shape as SSBS which could be due to splicing problems (single mode – to - helical cable).

To convert strain-rate DAS signals to equivalent geophone velocity signals it is required to have a prior knowledge of the P-wave velocity structure (compressional wave propagating along the fibre optic line) underneath the survey line. At the site we do not have prior information of velocity structure of the site. An alternative is to estimate the first P-wave arrival from DAS data, which however, it is not clearly observed in the collected wavefield. Thus, our approach is to select those scaling factors for all accelerometer positions that provide the same cross-correlation coefficient of 1.0 for all pair of DAS and accelerometer signals. The resulting values would be equivalent to the average velocity (Vp) structure underneath every accelerometer position, which can be latter compared to estimated velocity structure from the dispersion analysis (e.g. multiplying S-wave velocity by an appropriate Poisson's ratio).

The dispersion analysis is carried was carried out utilizing both active and passive collected records. Ideally, a combined passive + active dispersion curve should provide a reliable velocity model at the site. However, the combined image depicted an inconsistent dispersion pattern caused, apparently, by the overestimated phase velocity values (due to offline source position) compared to those values observed in the passive dispersion image.

9 Conclusions

After presenting the results of this research, it is concluded that the particle velocity derived from DAS data provide a very similar waveform as the particle velocity derived from accelerometer data in a very narrow frequency band at which the maximum energy occurs. The required velocity structure appears to be consistent with the soil characteristics of the ground conditions at the test site. This result suggests that the derivation of the particle velocity from DAS data must be executed in two steps. Firstly, the dispersion curve must be derived and secondly, the particle velocity will be derived by using the dispersion curve.

With respect to the additional questions for this research, mentioned in Section 2.1, it is concluded that:

a The spatial sampling of 1.0 meter seems to provide rather consistent information, in terms of number of cycles and spectral energy as observed in accelerometer signals.

b The influence of the coiling has not yet been studied in sufficient detail.

c Coupling conditions of the fibre optic cable seems to affect the amplitude of the spectral shape, but not the frequency at which the maximum energy occurs.

Some additional findings, that should be paid attention to in future research:

- The observed similarities among the collected strain rate and acceleration waveforms appear to be source dependent. At all accelerometers for near source positions the energy occurred at different frequency band, while for the farest shot positions both DAS and accelerometers depicted a very similar shape with the strongest spectral energy a very similar frequency band.
- The phase velocity spectra using active and passive type source provided very consistent dispersion energy trend. The phase velocity spectra computed for impulsive source depicted very similar dispersion modes for several coupling cases, while for passive measurements only the record with the best coupling depicted a coherent dispersion pattern.
- The computed particle velocity from DAS data provides a very similar waveform as computed velocity from accelerometer data in a very narrow frequency band at which the maximum energy occurs. The required velocity structure appears to be consistent with the soft soil characteristics of the ground conditions at the test site.

References

Ajo-Franklin, J. B., Dou, S., Lindsey, N. J., Monga, I., Tracy, C., Robertson, M., . . . Daley, T. J. S. r. (2019). Distributed acoustic sensing using dark fiber for near-surface characterization and broadband seismic event detection. *9*(1), 1-14.

Bakku, S. K. (2015). *Fracture characterization from seismic measurements in a borehole.* Massachusetts Institute of Technology.

Daley, T., Miller, D., Dodds, K., Cook, P., & Freifeld, B. J. G. P. (2016). Field testing of modular borehole monitoring with simultaneous distributed acoustic sensing and geophone vertical seismic profiles at Citronelle, Alabama. *64*(5), 1318-1334.

Dou, S., Lindsey, N., Wagner, A. M., Daley, T. M., Freifeld, B., Robertson, M., . . . Ajo-Franklin, J. B. J. S. r. (2017). Distributed acoustic sensing for seismic monitoring of the near surface: A traffic-noise interferometry case study. *7*(1), 1-12.

Gabriels, P., Snieder, R., & Nolet, G. (1987). IN SITU MEASUREMENTS OF SHEAR-WAVE VELOCITY IN SEDIMENTS WITH HIGHER-MODE RAYLEIGH WAVES*. *Geophysical Prospecting, 35*(2), 187-196. doi:10.1111/j.1365-2478.1987.tb00812.x

Lindsey, N. J., Martin, E. R., Dreger, D. S., Freifeld, B., Cole, S., James, S. R., . . . Ajo-Franklin, J. B. J. G. R. L. (2017). Fiber-optic network observations of earthquake wavefields. *44*(23), 11,792-711,799.

Park, C. B., Miller, R. D., & Xia, J. (1998). Imaging dispersion curves of surface waves on multi-channel records *In: Technical Program with biographies, SEG, 68th Annual Meeting, New Orleans, Expanded abstract, Society of Exploration Gephysicisits*, 1377-1380.

Park, C. B., Miller, R. D., & Xia, J. (1999). Multichannel analysis of surface waves. *Geophysics, 64*(3), 800–808.

Parker, T., Shatalin, S., & Farhadiroushan, M. J. f. b. (2014). Distributed Acoustic Sensing–a new tool for seismic applications. *32*(2), 61-69.

Shragge, J., Yang, J., Issa, N. A., Roelens, M., Dentith, M., & Schediwy, S. (2019). Low-frequency ambient Distributed Acoustic Sensing (DAS): Useful for subsurface investigation? In *SEG Technical Program Expanded Abstracts 2019* (pp. 963-967): Society of Exploration Geophysicists.

Tribaldos, V. R., Ajo-Franklin, J., Dou, S., Lindsey, N., Ulrich, C., Robertson, M., . . . Tracy, C. Surface Wave Imaging using Distributed Acoustic Sensing Deployed on Dark Fiber: Moving Beyond High Frequency Noise.

Wang, H. F., Zeng, X., Miller, D. E., Fratta, D., Feigl, K. L., Thurber, C. H., & Mellors, R. J. J. G. J. I. (2018). Ground motion response to an ML 4.3 earthquake using co-located distributed acoustic sensing and seismometer arrays. *213*(3), 2020-2036.

Appendix

Accelerometer channel	Name	Component	Position
01	TC1-1	X	1
02	TC1-2	Z	1
03	TC1-3	Y	1
04	V5	Z	2
05	V6	Y	2
06	TC3-1	X	3
07	TC3-2	Z	3
08	TC3-3	Y	3
09	V7	Z	4
10	V9	Y	4
11	TC4-1	X	5
12	TC4-2	Z	5
13	TC4-3	Y	5
14	V10	Z	6
15	V11	Y	6
16	TC5-1	X	7
17	TC5-2	Z	7
18	TC5-3	Y	7

Deltares is an independent institute for applied research in the field of water and subsurface. Throughout the world, we work on smart solutions for people, environment and society.